Machine Learning for Glaucoma Assessment using Fundus Images

Andres Diaz-Pinto
a.diaz-pinto@leeds.ac.uk

Outline

1. Introduction
2. Segmentation Methods
3. Classification Methods
4. Image synthesis
5. Conclusions

Outline

1. **Introduction**
   - **Motivation**
   - Anatomy of the retina
   - Types of glaucoma
   - Imaging technology
   - Objectives
2. Segmentation Methods
3. Classification Methods
4. Image synthesis
5. Conclusions

Motivation

→ Glaucoma is the second most common cause of blindness worldwide, according to the World Health Organization (United Nations agency).

→ It affects more than 60 million people.

Motivation

<u>Early detection and treatment is important to prevent vision loss.</u>

HOWEVER, screening to large population is expensive.

FOR THAT REASON, the development of automatic glaucoma assessment algorithms is of great interest.

Outline

1. **Introduction**
   - Motivation
   - **Anatomy of the retina**
   - Types of glaucoma
   - Imaging technology
   - Objectives
2. Segmentation Methods
3. Classification Methods
4. Image synthesis
5. Conclusions

Anatomy of the retina

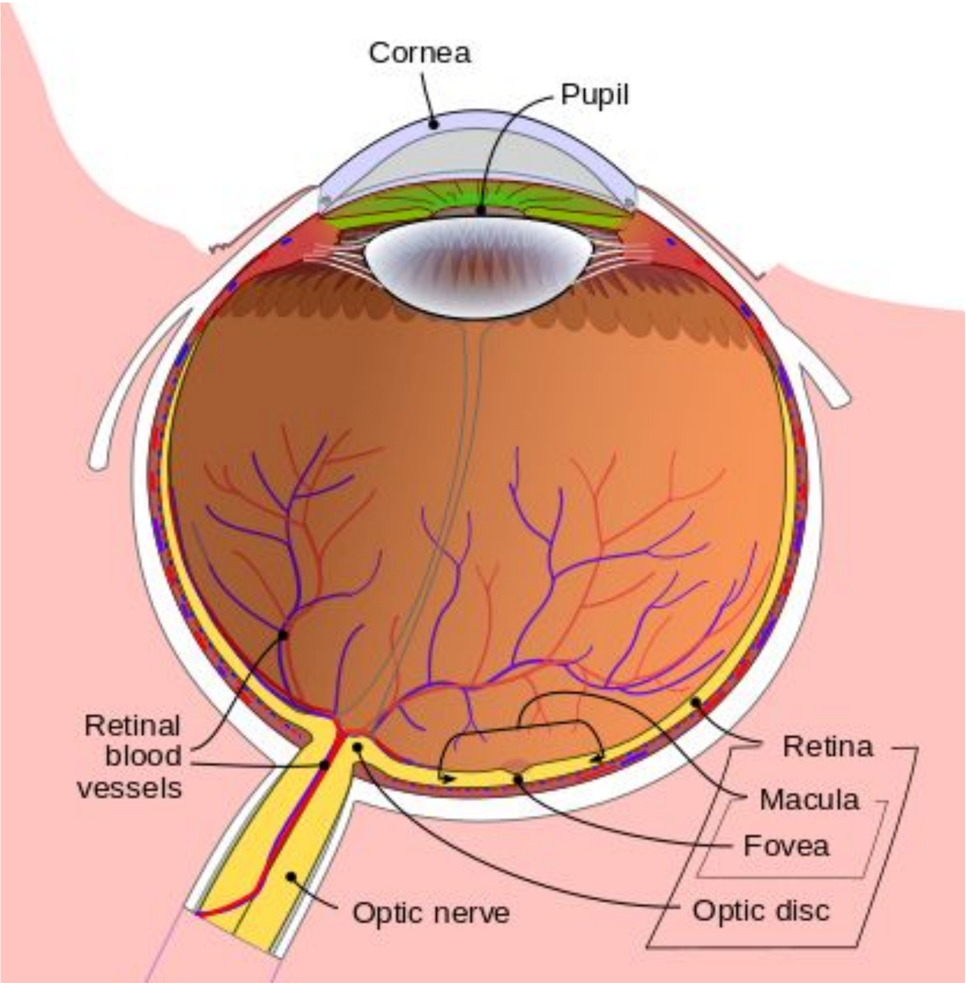

Three main structures:

- The optic disc
- Retinal blood vessels
- The macula

Anatomy of the retina

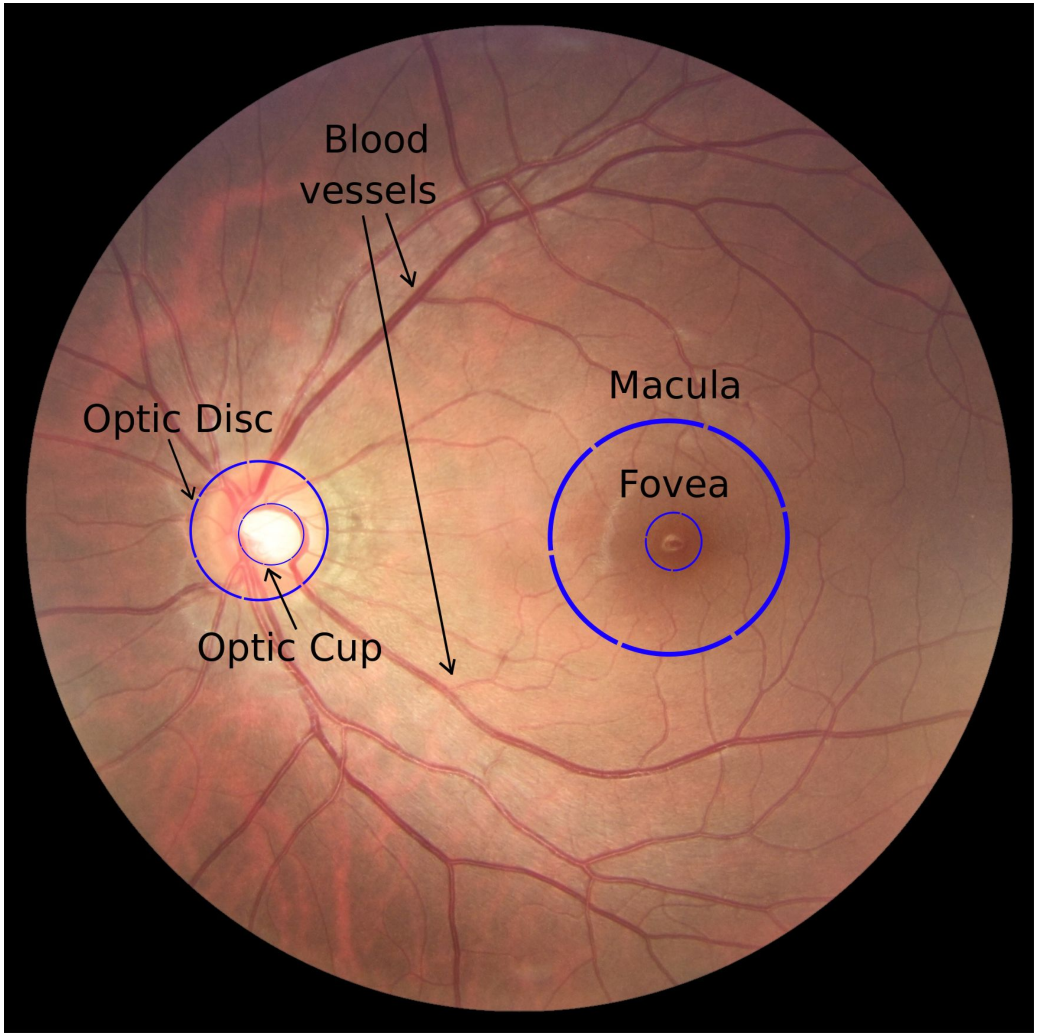

Outline

1. **Introduction**
   - Motivation
   - Anatomy of the retina
   - **Types of glaucoma**
   - Imaging technology
   - Objectives
2. Segmentation Methods
3. Classification Methods
4. Image synthesis
5. Conclusions

Types of glaucoma

Glaucoma refers to a deepening or excavation of the optic nerve head.

And there are three main forms of glaucoma:

1. Open-angle glaucoma
2. Angle closure glaucoma and
3. Congenital glaucoma

Types of glaucoma

1. Open-angle glaucoma

   Also called **primary or chronic glaucoma**

   It is the most common type of glaucoma (at least 90% of all glaucoma cases)

   Slow clogging of the drainage canals

Types of glaucoma

2. Angle closure glaucoma

It is a less common form of glaucoma

It is caused by blocked drainage canals

Types of glaucoma

Open- and closure-angle glaucoma differences

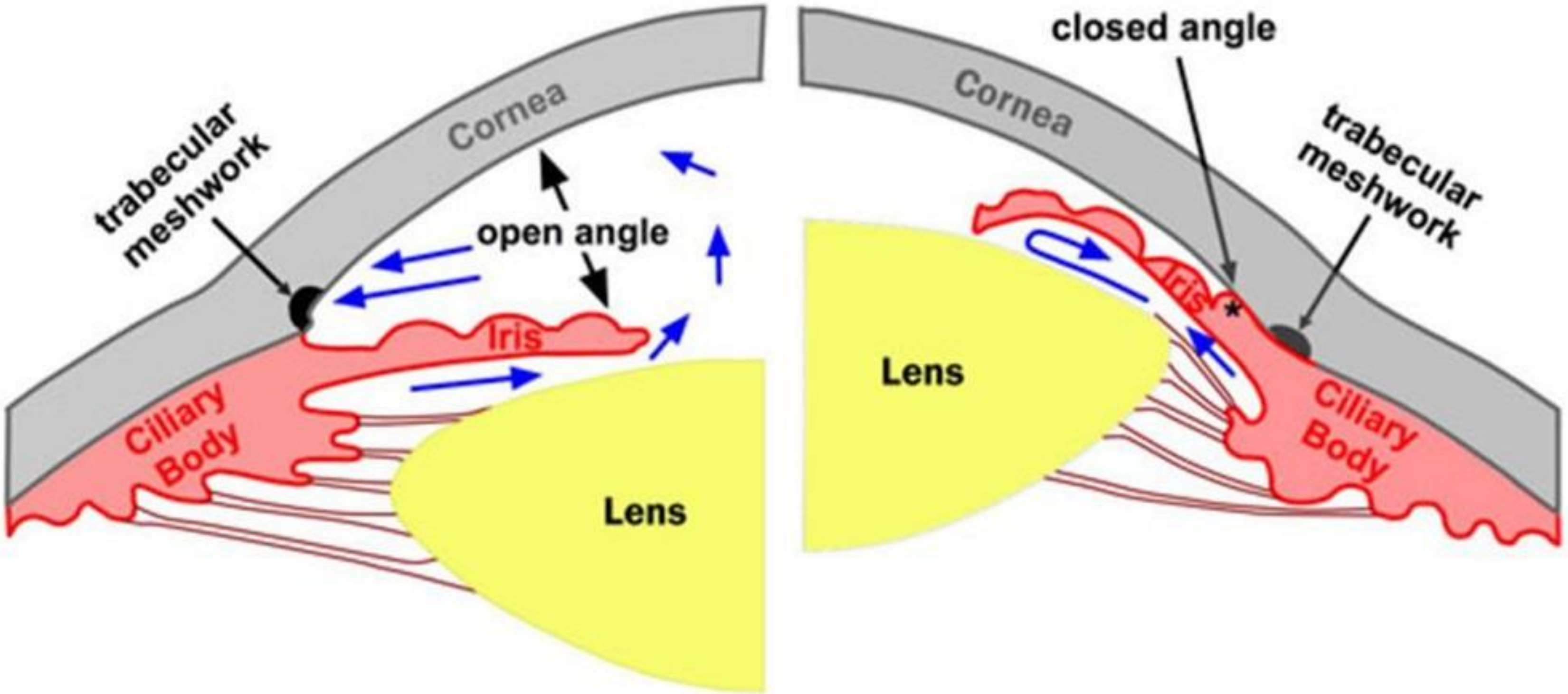

Types of glaucoma

3. Congenital glaucoma

Rare condition that may be inherited

Occurs in babies when there is incorrect or incomplete development of the eye's drainage canals

Outline

1. **Introduction**
   - Motivation
   - Anatomy of the retina
   - Types of glaucoma
   - **Imaging technology**
   - Objectives
2. Segmentation Methods
3. Classification Methods
4. Image synthesis
5. Conclusions

Imaging technology

1. Fundus photograph

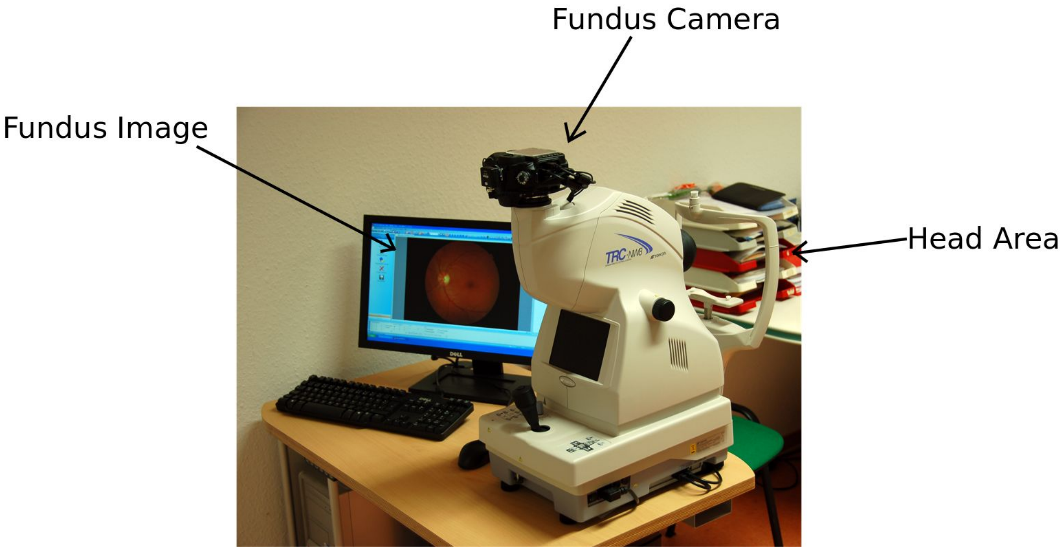

Imaging technology

2. Optical Coherence Tomography (OCT)

Backscattered light depicts variations in optical reflectance (A-scan)

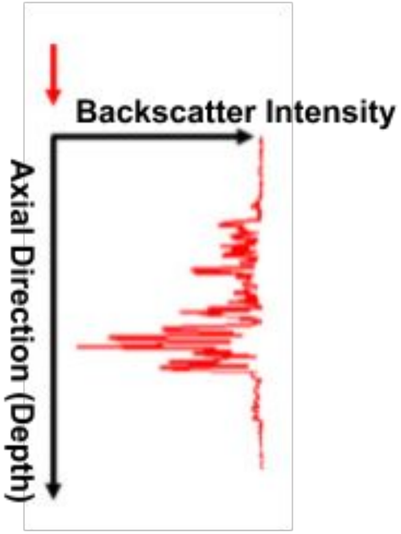

A-scan

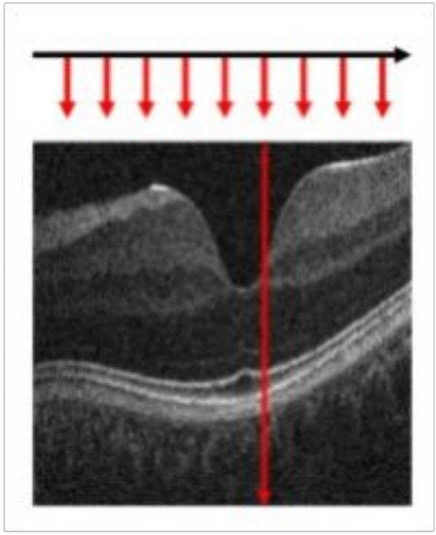

B-scan

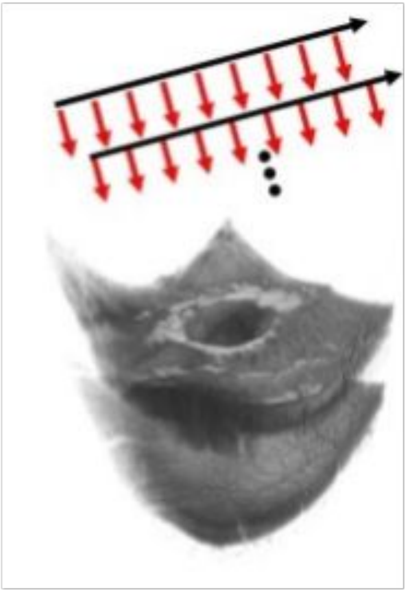

C-scan

Imaging technology

Main differences:

Fundus Photograph	**OCT**
RGB image	Tomography (up to 3D image)
Less accurate measurements	High accurate measurements
Low cost	Prohibitively expensive for mass screening

Outline

1. **Introduction**
   - Motivation
   - Anatomy of the retina
   - Types of glaucoma
   - Imaging technology
   - **Objectives**
2. Segmentation Methods
3. Classification Methods
4. Image synthesis
5. Conclusions

Objectives

- To **study the state-of-the-art** of segmentation techniques and automatic glaucoma assessment algorithms using retinal fundus images.

- To propose **new algorithms to segment and extract clinical features** using retinal fundus images with the aim of automatically detecting glaucoma.

- Development and **implementation of algorithms based on machine learning and/or deep learning** that help ophthalmologists to detect glaucoma by using retinal fundus images.

Outline

1. Introduction
2. **Segmentation Methods**
   - **Stochastic-Watershed-based method**
   - U-Net-based approach
   - Conclusions
3. Classification Methods
4. Image synthesis
5. Conclusions

Rationale

Segment important parts of the retina to measure clinical features

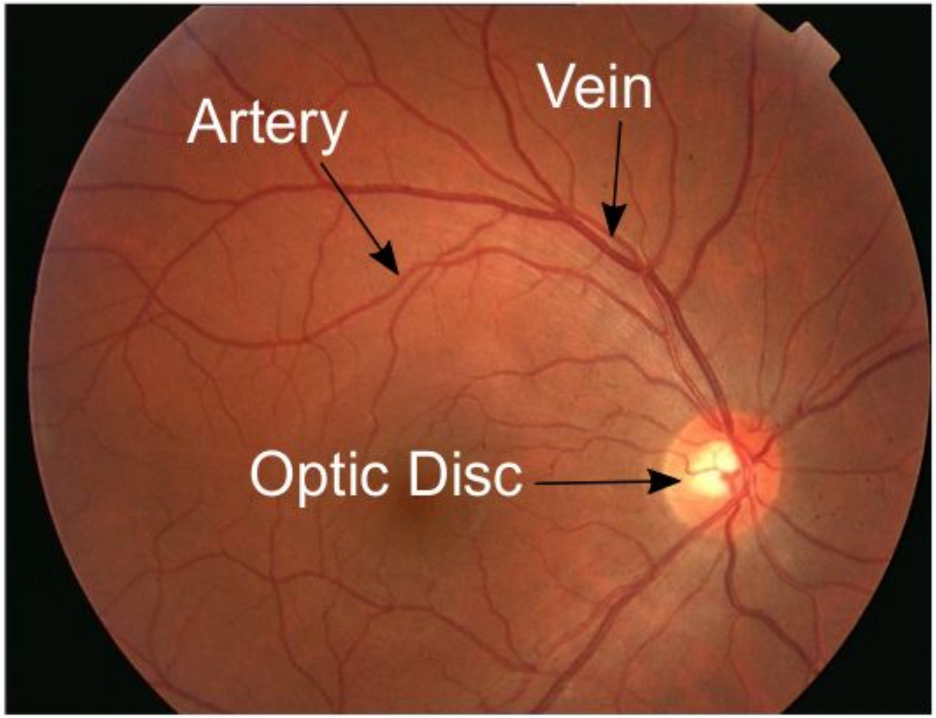

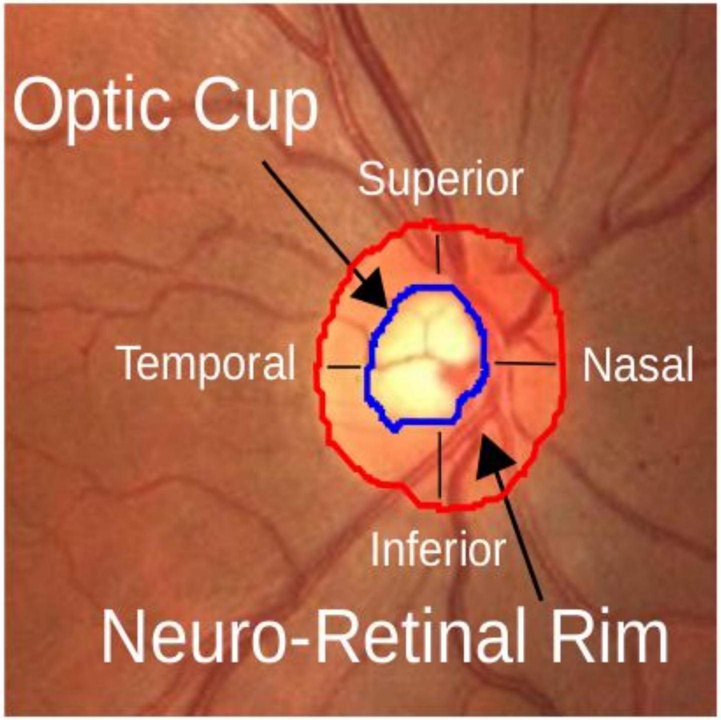

Stochastic-Watershed-based method

FIRST, regular Watershed transformation

- Convert in grayscale

  Minimum pixel values -> object of interest

  Maximum pixel values -> separation boundaries

- Use gradient magnitude

- Assign markers

- Compute the watershed transform

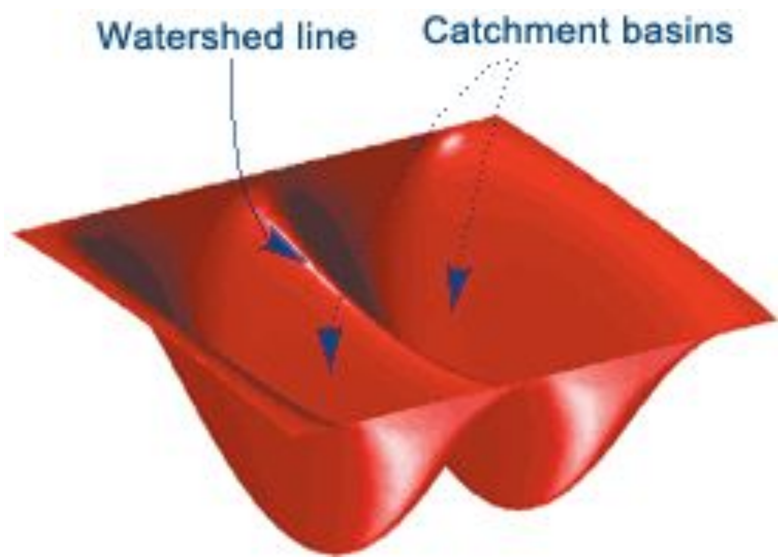

Image taken from https://uk.mathworks.com/company/newsletters/articles/the-watershed-transform-strategies-for-image-segmentation.html

Stochastic-Watershed-based method

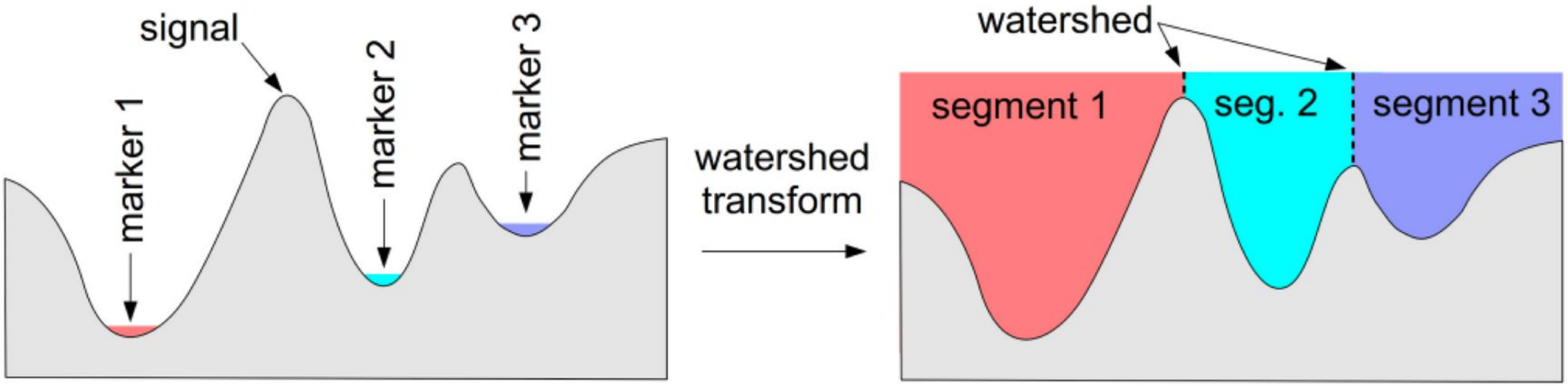

Regular Watershed transformation

Image taken from https://res.mdpi.com/remotesensing/remotesensing-06-00776/article_deploy/html/images/remotesensing-06-00776f3.png

Stochastic-Watershed-based method

Over- and under-segmentation problems!

Marker-controlled watershed:

- Uses of internal and external markers
- External markers limits the segmented area
- Internal markers follow a Poisson distribution

Stochastic-Watershed-based method

How it works?

- M marker-controlled watershed realizations
- The idea is to estimate a probability density function (pdf) for the contours of the image

  It filters out non-significant border fluctuations

- Additional last marker-controlled on the obtained pdf

Stochastic-Watershed-based method

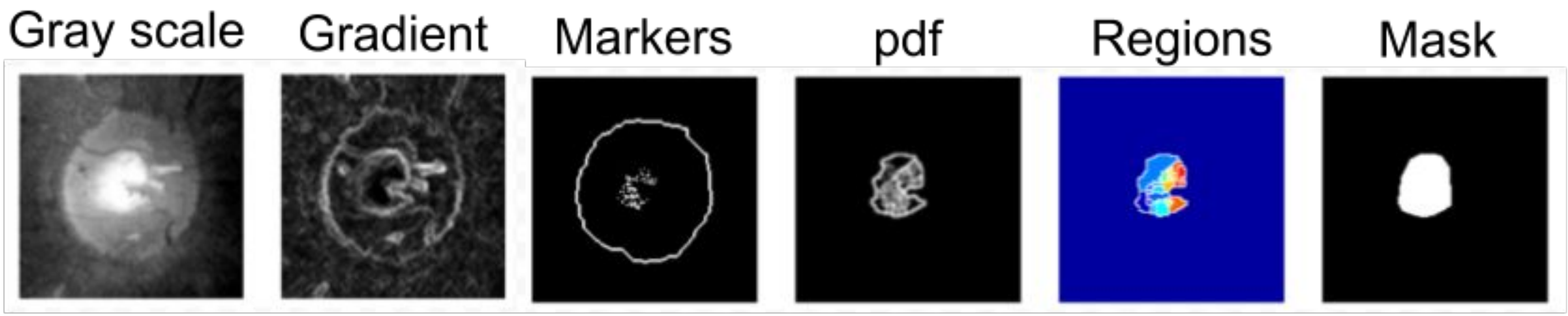

Stochastic-Watershed-based method

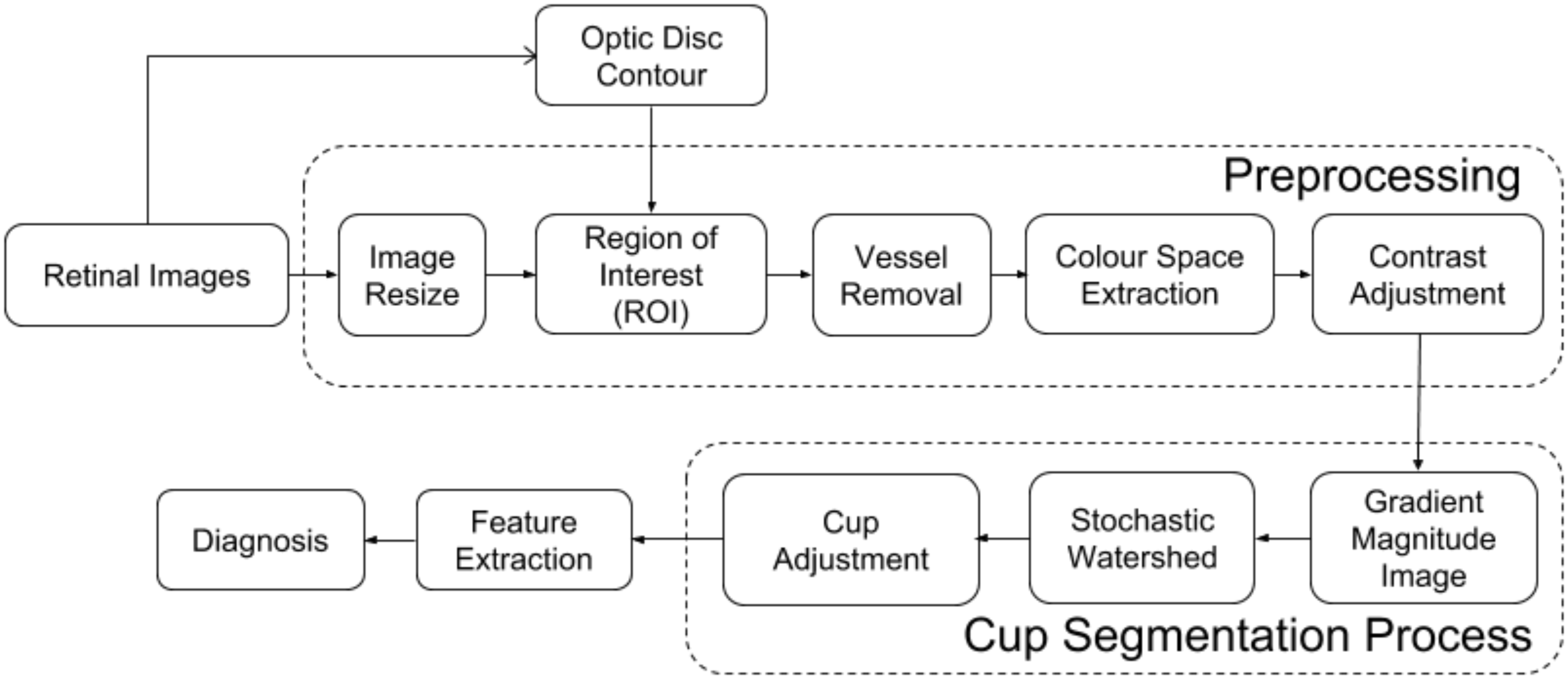

Stochastic-Watershed-based method

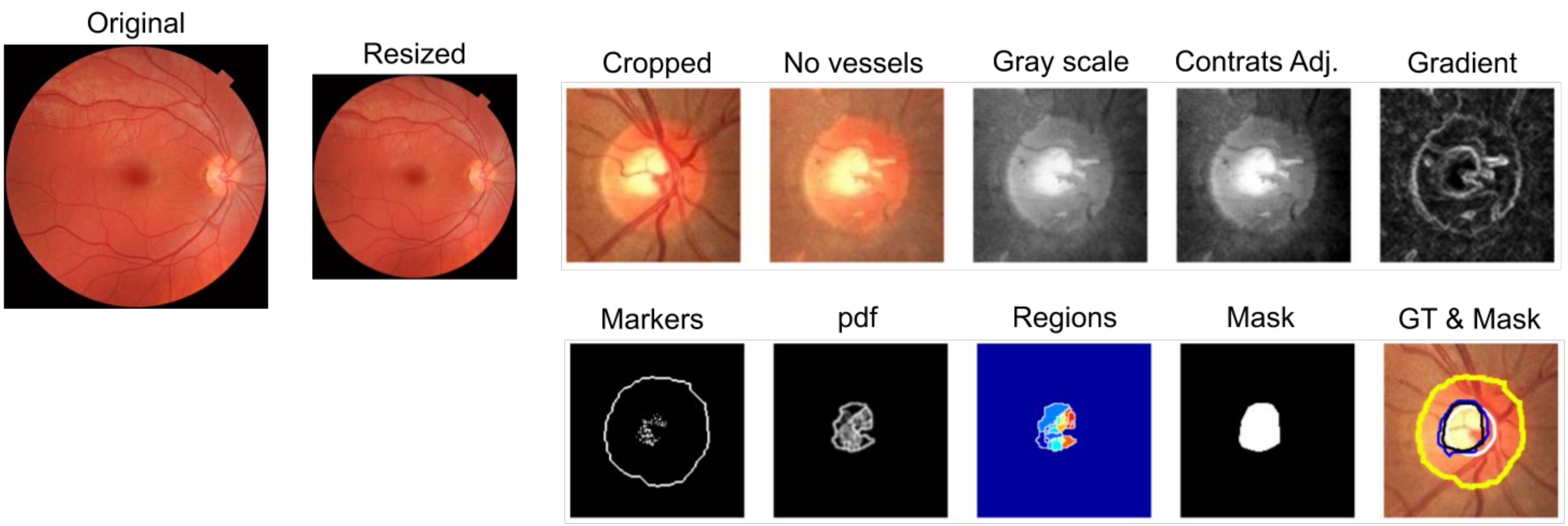

Stochastic-Watershed-based method

Databases

Name	# of Images	Glaucoma	Normal
12Octubre	53	29	24
Drive	40	20	20
Drishti-GS1	101	70	31
Autogla	83	50	33
HRF	45	27	18
RIM-ONE	401	150	251
Total	**723**	**346**	**377**

Stochastic-Watershed-based method

Component Analysis

Database	Index	CMYK	YIQ	Luv	Lab	PCA	RGB
12Octubre	Jaccard	$0,553 \pm 0,185$	$0,565 \pm 0,215$	$0,526 \pm 0,260$	$0,551 \pm 0,238$	$0,558 \pm 0,214$	$\mathbf{0,575 \pm 0.192}$
	Dice	$0,692 \pm 0,173$	$0,695 \pm 0,204$	$0,643 \pm 0,281$	$0,674 \pm 0,250$	$0,689 \pm 0,202$	$\mathbf{0,709 \pm 0.178}$
DRIVE	Jaccard	$\mathbf{0,567 \pm 0,198}$	$0,481 \pm 0,227$	$0,415 \pm 0,247$	$0,461 \pm 0,224$	$0,471 \pm 0,211$	$0,495 \pm 0.200$
	Dice	$\mathbf{0,700 \pm 0,191}$	$0,615 \pm 0,233$	$0,541 \pm 0,269$	$0,596 \pm 0,239$	$0,611 \pm 0,209$	$0,638 \pm 0.187$
Drishti-GS1	Jaccard	$0,656 \pm 0.191$	$0,661 \pm 0.215$	$0,347 \pm 0.350$	$0,492 \pm 0.328$	$\mathbf{0,668 \pm 0.200}$	$0,664 \pm 0.185$
	Dice	$0,775 \pm 0.160$	$0,771 \pm 0.190$	$0,416 \pm 0.391$	$0,583 \pm 0.356$	$\mathbf{0,781 \pm 0.175}$	$0,780 \pm 0.161$
Autogla	Jaccard	$0,568 \pm 0,197$	$0,551 \pm 0,210$	$0,512 \pm 0,270$	$0,527 \pm 0,240$	$0,560 \pm 0,209$	$\mathbf{0,572 \pm 0.201}$
	Dice	$0,702 \pm 0,177$	$0,683 \pm 0,207$	$0,626 \pm 0,296$	$0,653 \pm 0,245$	$0,693 \pm 0,194$	$\mathbf{0,706 \pm 0.180}$
HRF	Jaccard	$0,607 \pm 0,185$	$\mathbf{0,627 \pm 0,150}$	$0,545 \pm 0,250$	$0,592 \pm 0,221$	$0,575 \pm 0,212$	$0,614 \pm 0.179$
	Dice	$0,738 \pm 0,161$	$\mathbf{0,759 \pm 0,131}$	$0,663 \pm 0,269$	$0,712 \pm 0,234$	$0,704 \pm 0,199$	$0,744 \pm 0.161$
RIM-ONE	Jaccard	$0,523 \pm 0,190$	$\mathbf{0,540 \pm 0,178}$	$0,329 \pm 0,287$	$0,464 \pm 0,253$	$0,491 \pm 0,209$	$0,515 \pm 0.198$
	Dice	$0,665 \pm 0,175$	$\mathbf{0,683 \pm 0,169}$	$0,423 \pm 0,336$	$0,586 \pm 0,281$	$0,630 \pm 0,202$	$0,656 \pm 0.185$
All databases	Jaccard	$0,559 \pm 0,203$	$\mathbf{0,565 \pm 0,218}$	$0,546 \pm 0,259$	$0,468 \pm 0,233$	$0,546 \pm 0,227$	0.537 ± 0.205
	Dice	$0,696 \pm 0,187$	$\mathbf{0,702 \pm 0,221}$	$0,679 \pm 0,281$	$0,590 \pm 0,226$	$0,682 \pm 0,215$	0.674 ± 0.190

Stochastic-Watershed-based method

Comparison with other methods

	$E <= 0,1$	$E <= 0,2$	$E <= 0,3$	$E <= 0,4$	$E <= 0,5$	μ_E	Images used
Thresholding [9]	0 %	3 %	15 %	31 %	47 %	53,50 %	138
R-bend [27]	0 %	4 %	28 %	56 %	77 %	39,50 %	200
Proposed method	**1** %	**10** %	**30** %	**50** %	**69** %	**41.06** %	**723**
ASM [28]	3 %	25 %	51 %	76 %	88 %	31,30 %	325
Regression [29] [30]	6 %	29 %	62 %	81 %	95 %	28,40 %	650
Superpixel [8]	8 %	42 %	75 %	90 %	96 %	24,10 %	650

We used more images and from different centres!

Stochastic-Watershed-based method

Clinical features

Cup/Disc ratio (**CDR**): Vertical ratio between Cup and Disc

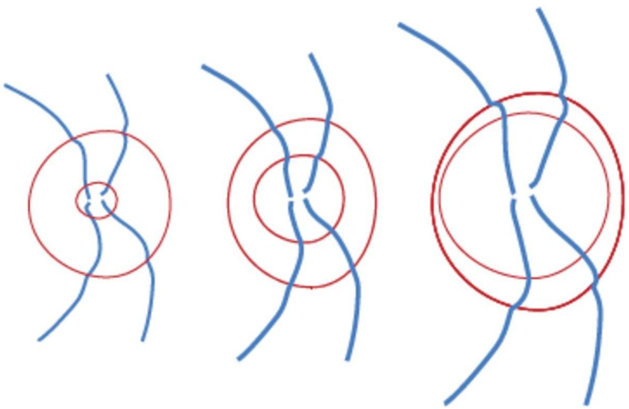

Area Cup/Disc ratio (**ACDR**): Ratio between area occupied by the Cup and the Disc

ISNT rule: Inferior > Superior > Nasal > Temporal
A normal eye follows this rule

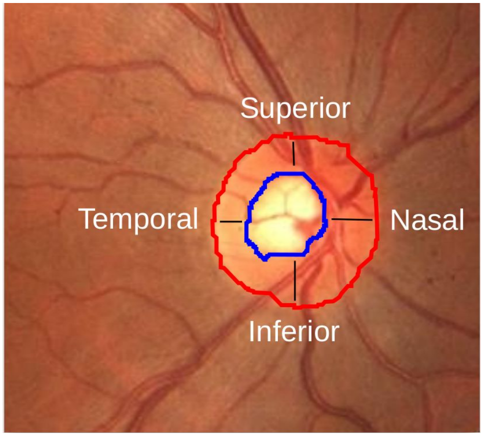

Stochastic-Watershed-based method

Glaucoma Diagnosis

	CMYK		YIQ		Luv		Lab		PCA		RGB	
	Sp	Se	Sp	Se	Sp	Se	Sp	Se	Sp	Se	Sp	Se
CDR	0,574	0,697	**0,675**	**0,674**	0,650	0,731	0,832	0,563	0,487	0,716	0.545	0.716
ACDR	0,601	0,633	**0,715**	**0,604**	0,688	0,673	0,849	0,509	0,517	0,663	0.574	0.655
ISNT	0,495	0,570	**0,431**	**0,568**	0,422	0,561	0,337	0,609	0,523	0,544	0.499	0.511
Combined	0,545	0,702	**0,730**	**0,602**	0,685	0,635	0,373	0,760	0,376	0,778	0.513	0.742

Combined means we used CDR and ISNT rule to assess glaucoma

Stochastic-Watershed-based method

Glaucoma Diagnosis

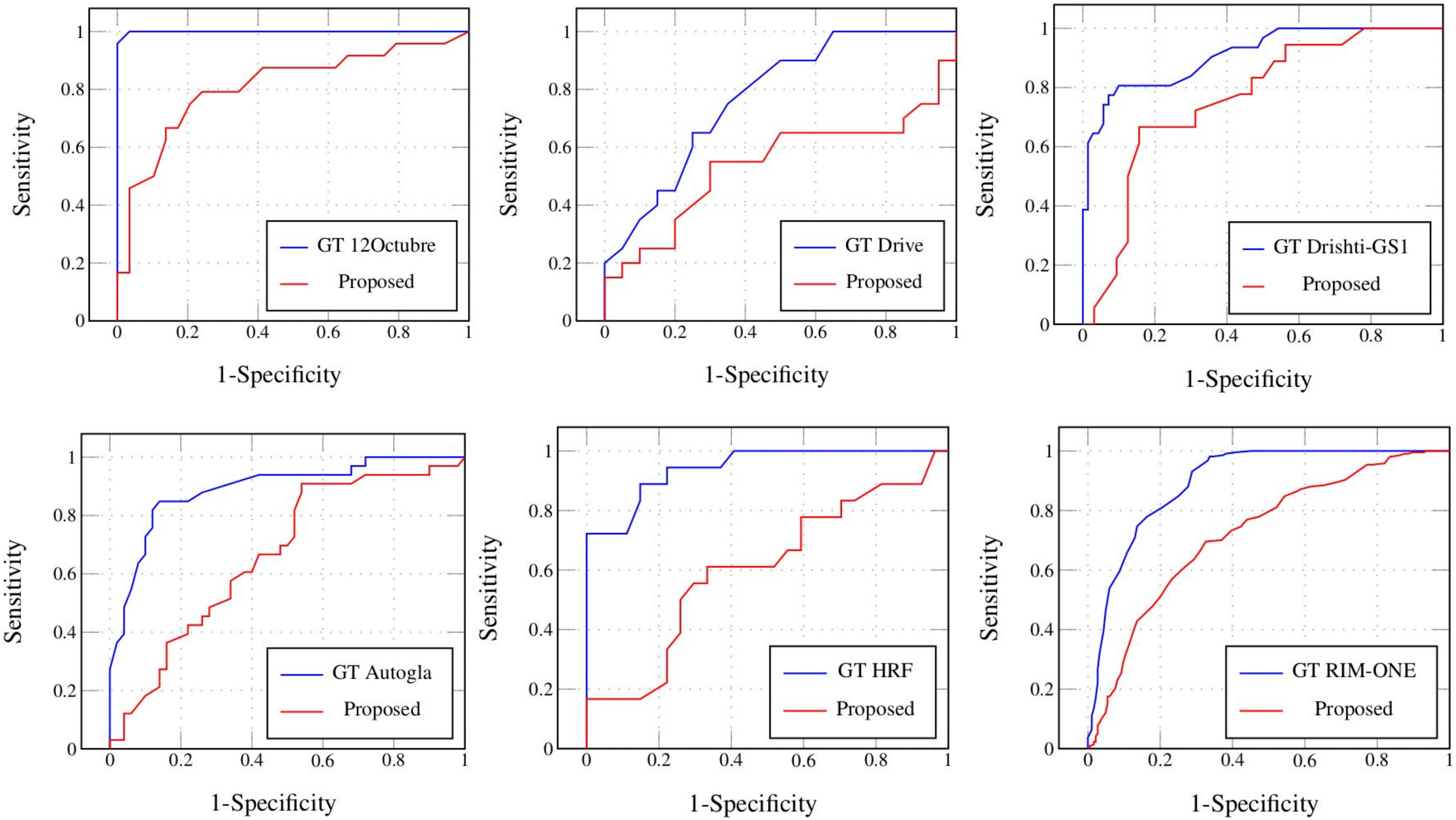

Stochastic-Watershed-based method

Glaucoma Diagnosis

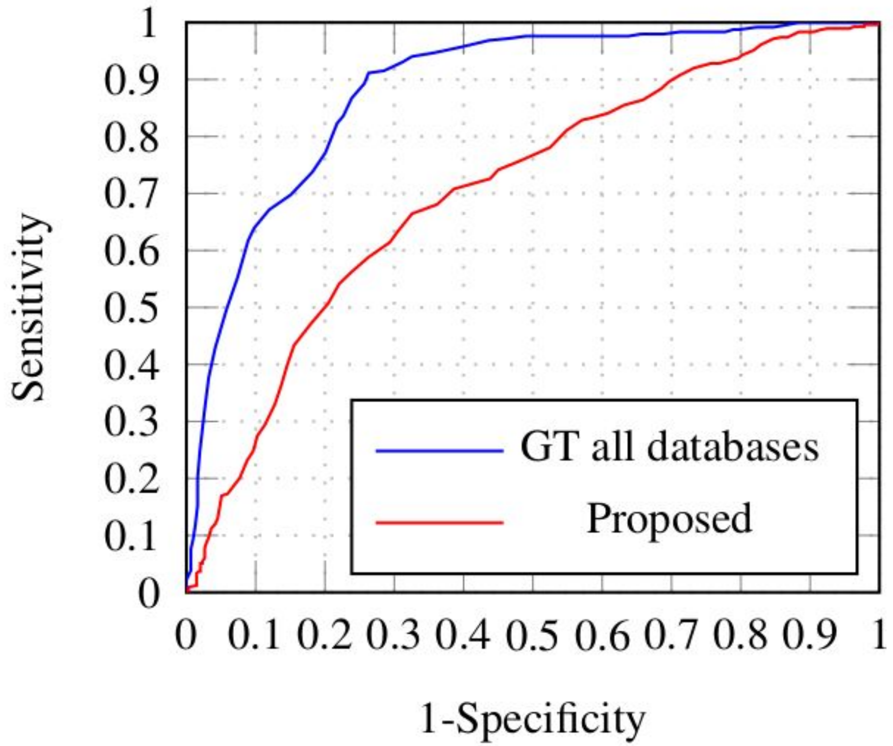

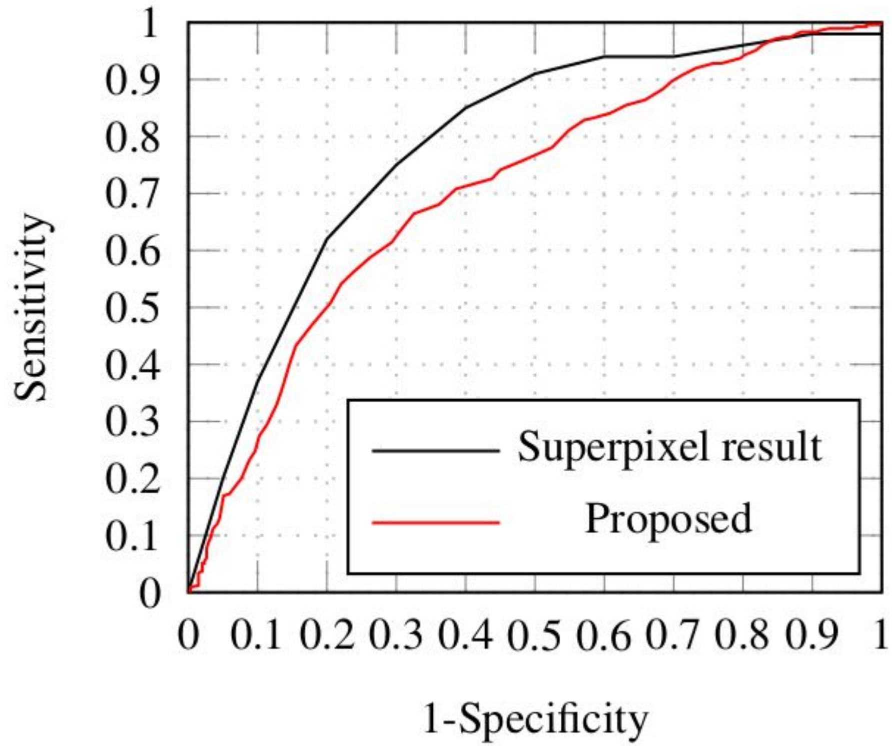

Outline

1. Introduction
2. **Segmentation Methods**
   - Stochastic-Watershed-based method
   - **U-Net-based approach**
   - Conclusions
3. Classification Methods
4. Image synthesis
5. Conclusions

U-Net-based approach

- Fully convolutional network
- The contracting path captures context.
- Symmetric expanding path enables precise localization.

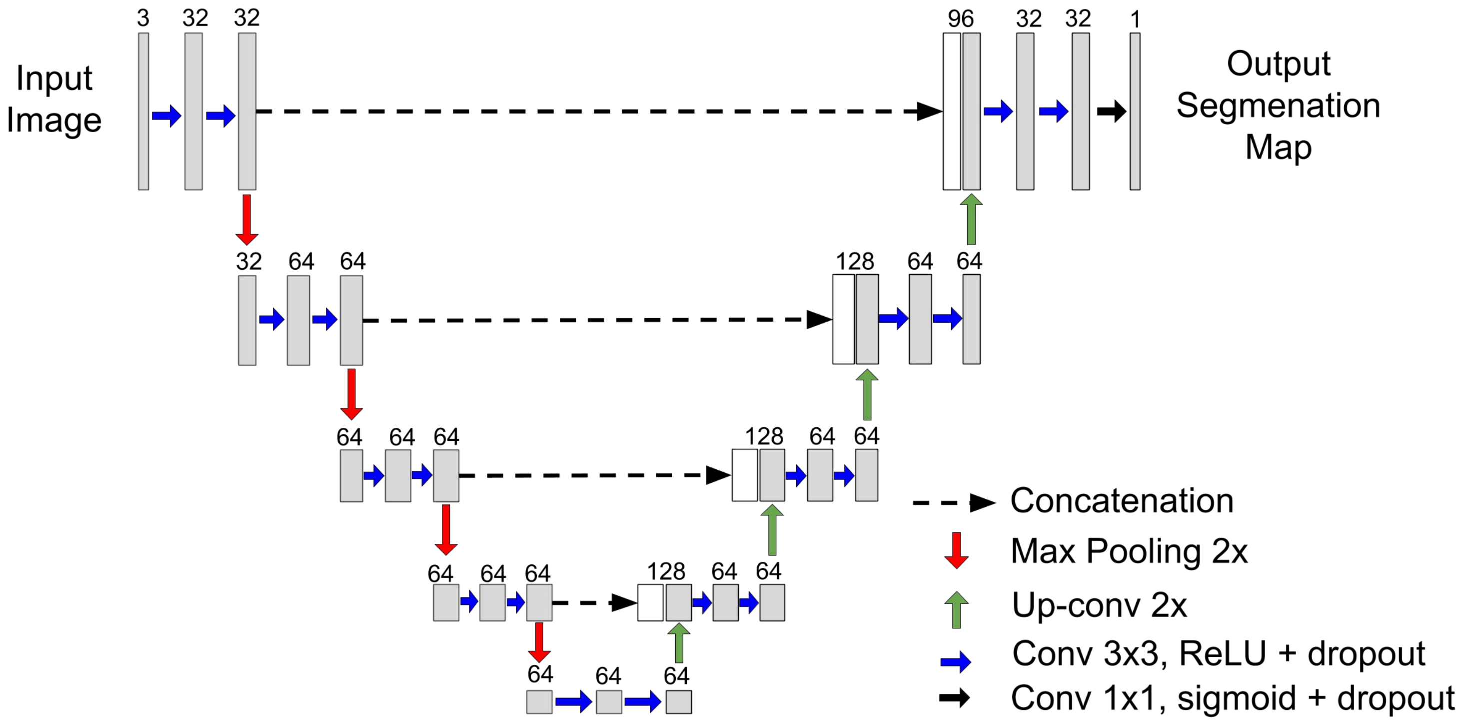

U-Net-based approach

- We used Contrast Limited Adaptive **Histogram Equalization (CLAHE)** as a preprocessing technique

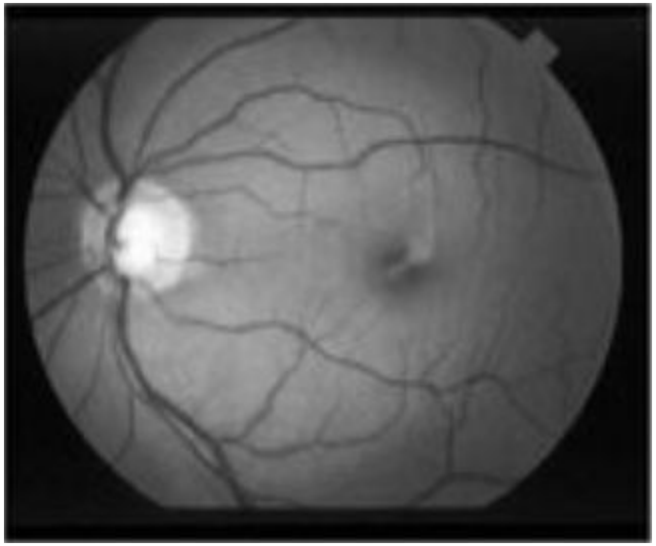

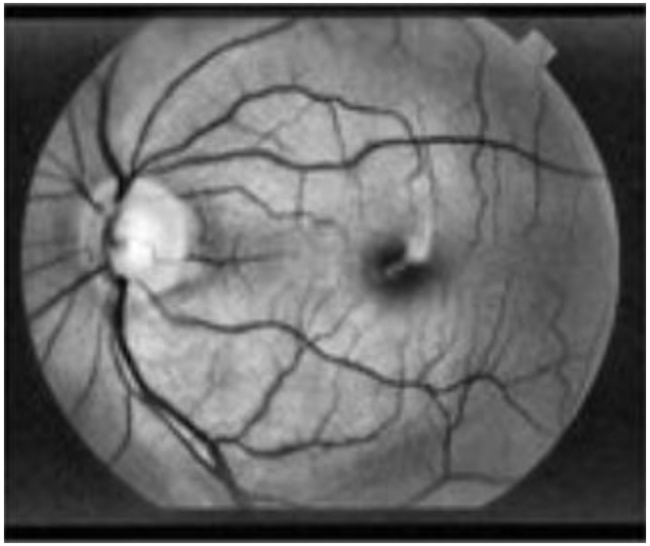

U-Net-based approach

- We applied data augmentation to use the available annotated samples more efficiently.

  Rotation, translation and zoom

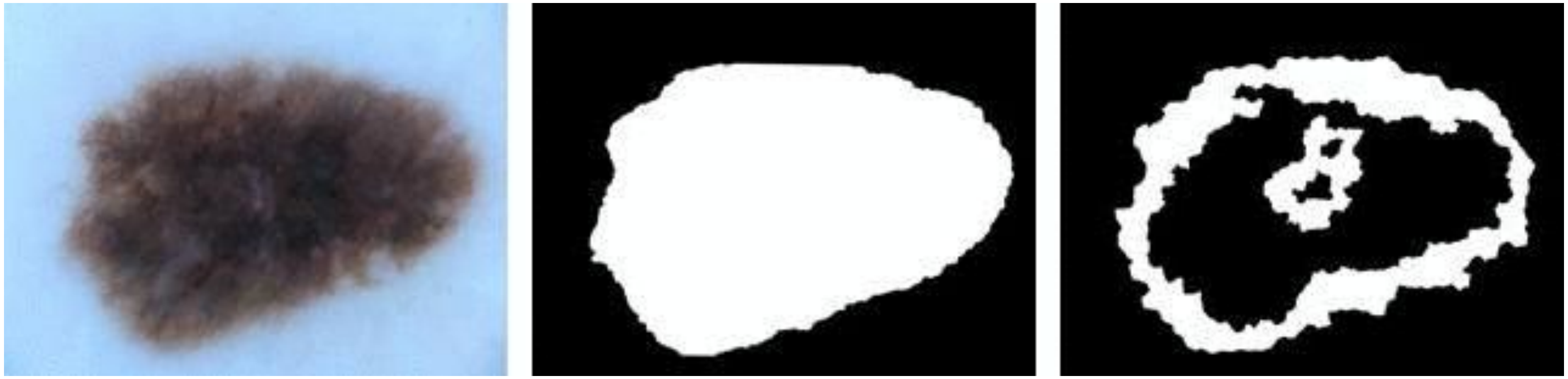

Image taken from: https://github.com/mdbloice/Augmentor

U-Net-based approach

Schema used for Optic Disc and Optic Cup segmentation

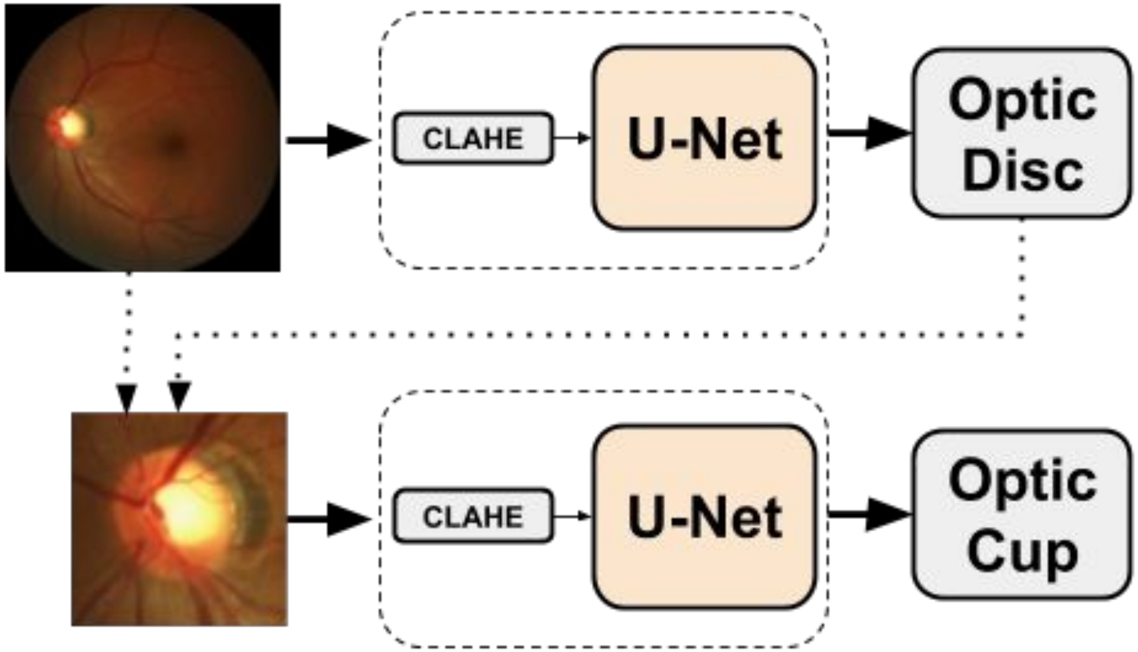

U-Net-based approach

Databases

Name	# of Images
DRIONS-DB	110
Drishti-GS1	101
REFUGE	400
Total	**611**

A Dice index of **0.91** and **0.78** were obtained for the optic disc and optic cup

U-Net-based approach

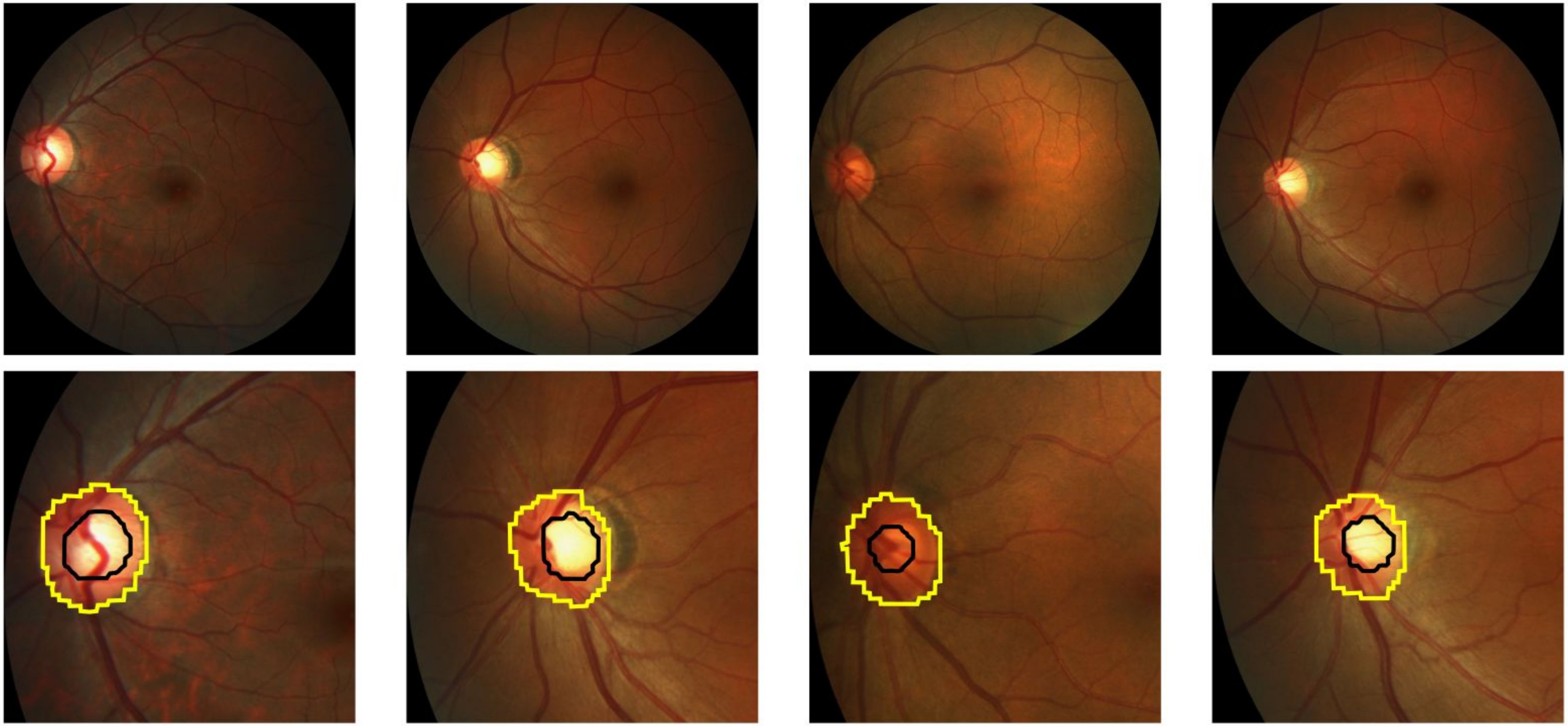

Outline

1. Introduction
2. **Segmentation Methods**
   - Stochastic-Watershed-based method
   - U-Net-based approach
   - **Conclusions**
3. Classification Methods
4. Image synthesis
5. Conclusions

Conclusions

Stochastic Watershed method:

- It is focused on measuring the clinical features such as CDR, ACDR and ISNT rule
- It is highly affected by the pallor presented in the optic cup (intensity).

U-Net method:

- It has the ability to learn more discriminative features than only the intensity.
- It is focused on Optic Disc and Optic Cup segmentation (REFUGE Challenge)

Results obtained from this approach are affected on how well the Cup and the Disc are segmented

Outline

1. Introduction
2. Segmentation Methods
3. **Classification Methods**
   - **ImageNet-trained CNN architectures**
   - Ensemble Setting with CNNs
   - Conclusions
4. Image synthesis
5. Conclusions

ImageNet-trained CNN architectures

ImageNet-trained CNN architectures applied for retinal image classification:

VGG16 and VGG19: These CNNs are based on the same model and characterized by their simplicity. Presented by Simonyan in 2014 for the ImageNet challenge

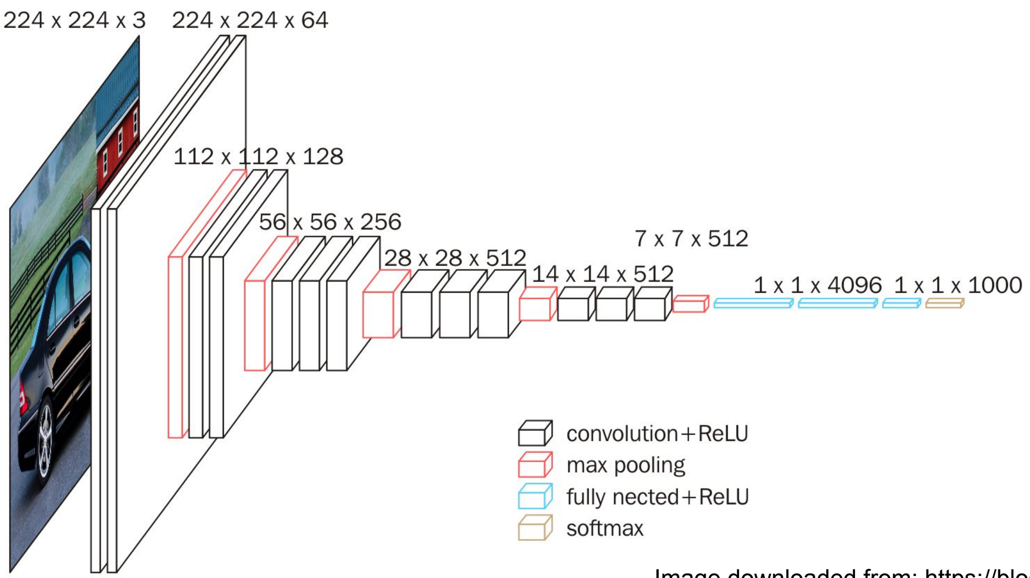

Image downloaded from: https://blog.datawow.io/cnn-models-ef356bc11032

ImageNet-trained CNN architectures

GoogLeNet: It was first introduced by Szegedy et al. in 2015. It is based on the Inception module.

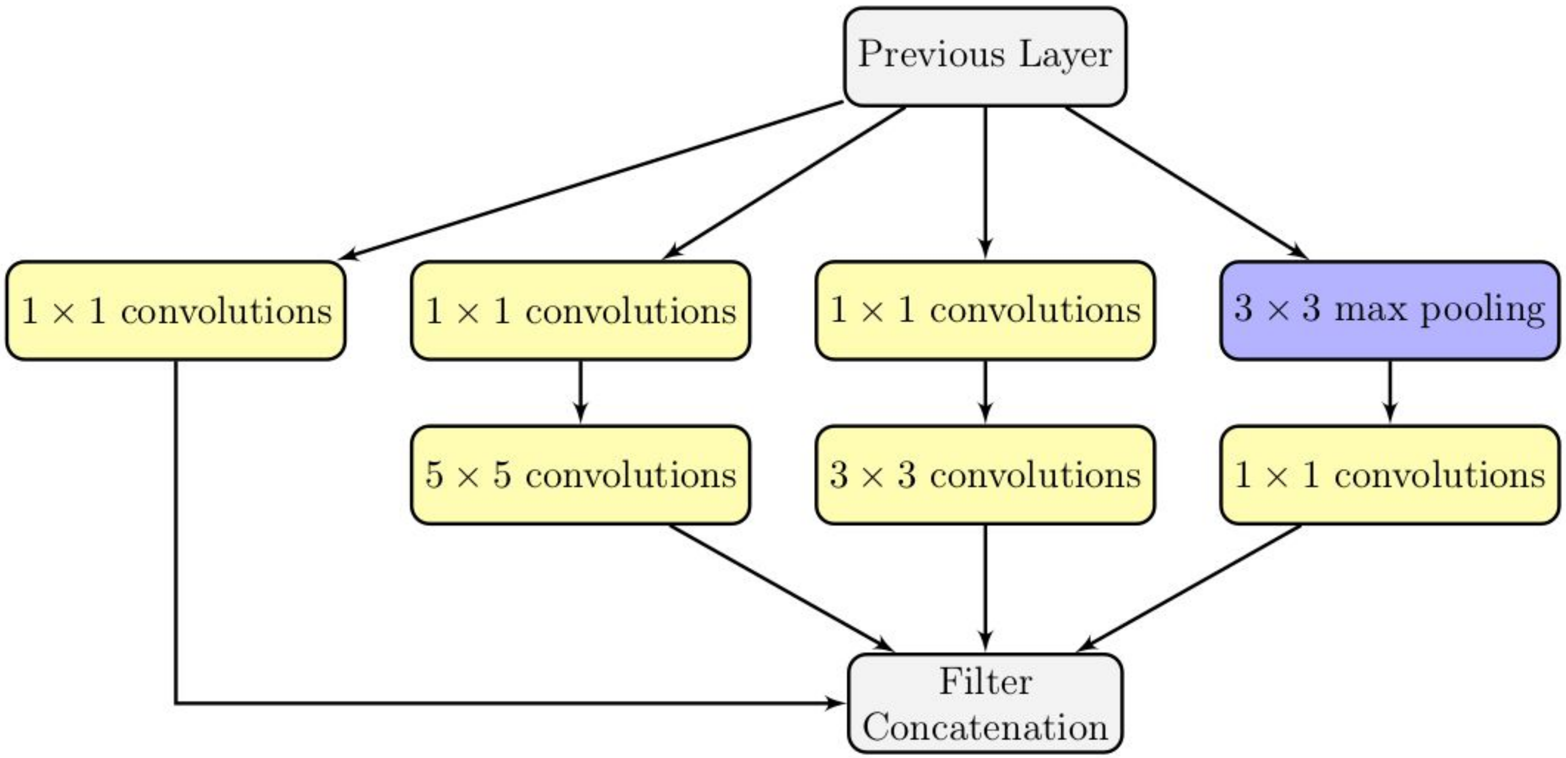

ImageNet-trained CNN architectures

Microsoft ResNet: This architecture was proposed by the Microsoft Research Asia team (MSRA) in 2015. It is considered an “exotic architecture” that relies on residual blocks.

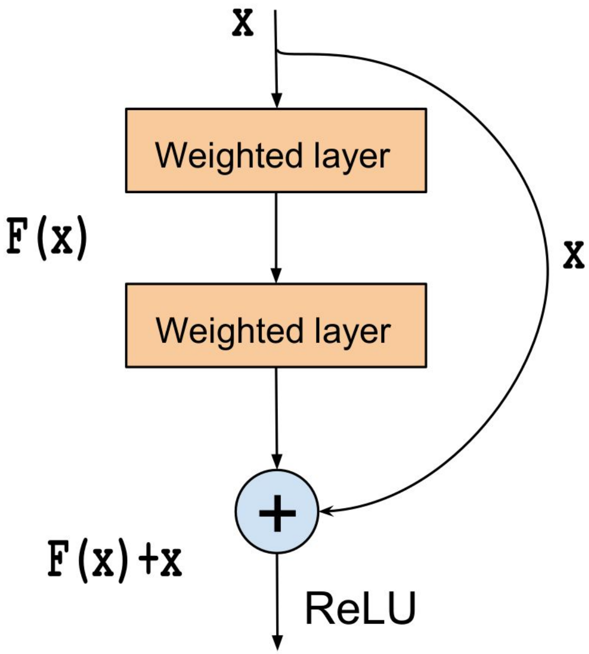

ImageNet-trained CNN architectures

Xception: or Extreme Inception, it was proposed by F. Chollet in 2016. It is an extension of the Inception architecture.

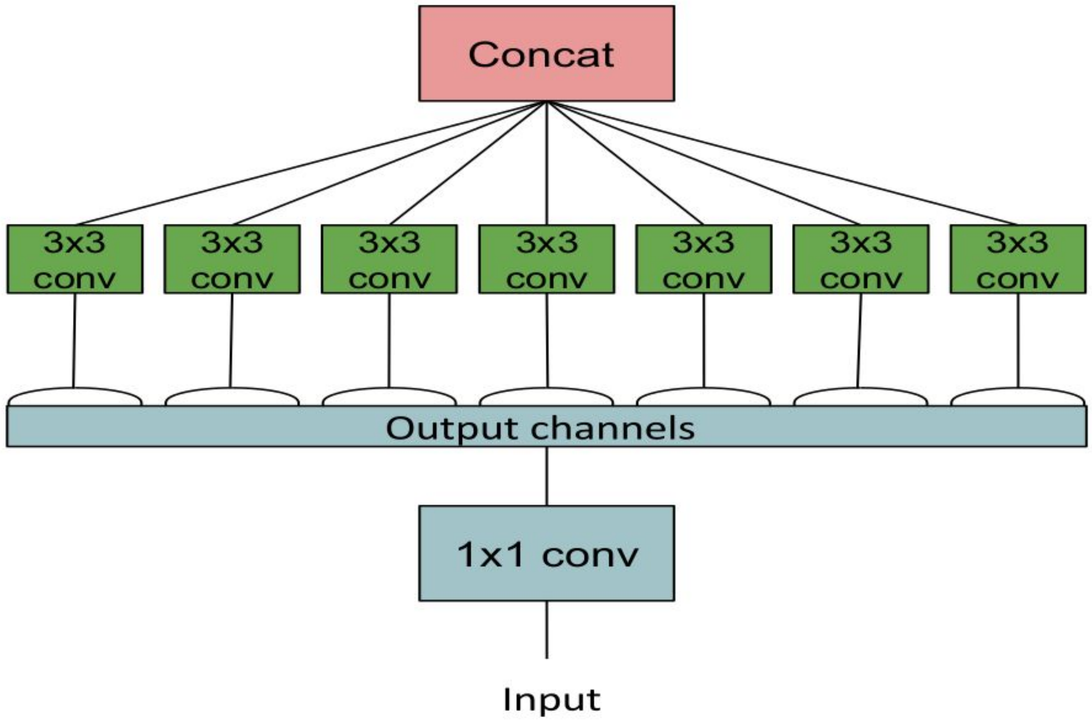

ImageNet-trained CNN architectures

Fine-tuning technique:

a) The weight initialization of the convolutional layers using the ImageNet weights and
b) The replacement of the classification function or the number of nodes in the last fully connected layer.

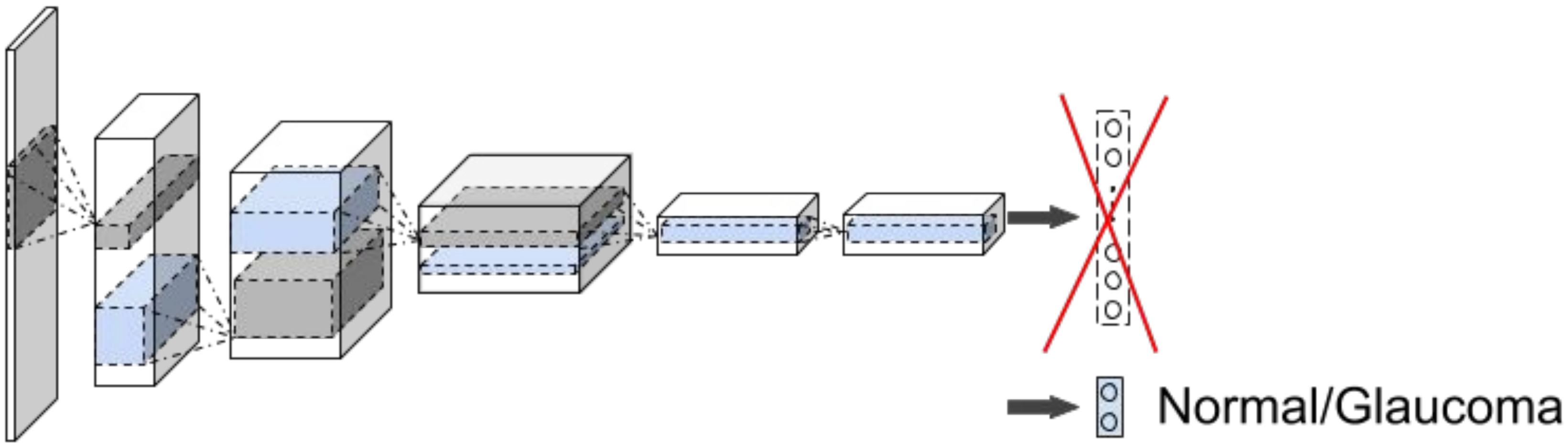

ImageNet-trained CNN architectures

Deep- or shallow tuning?

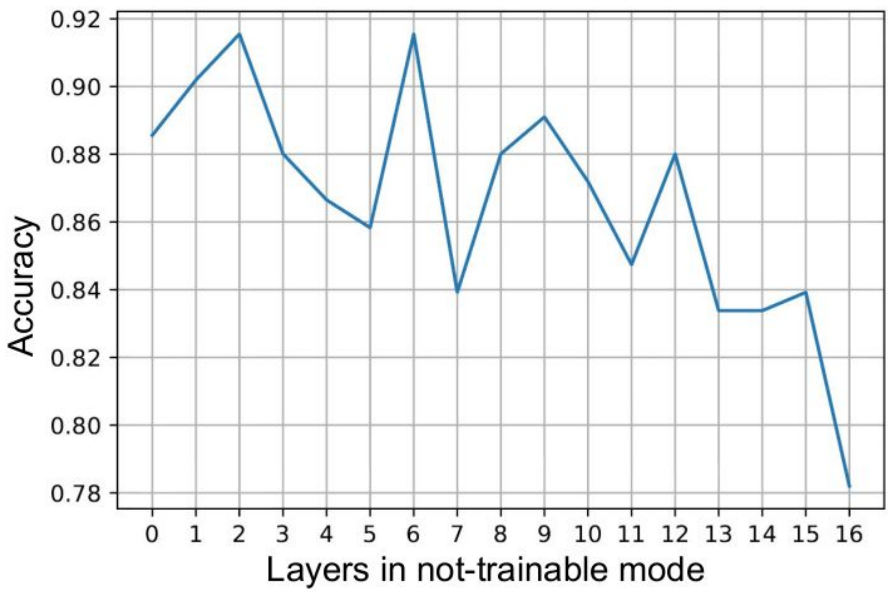

VGG16

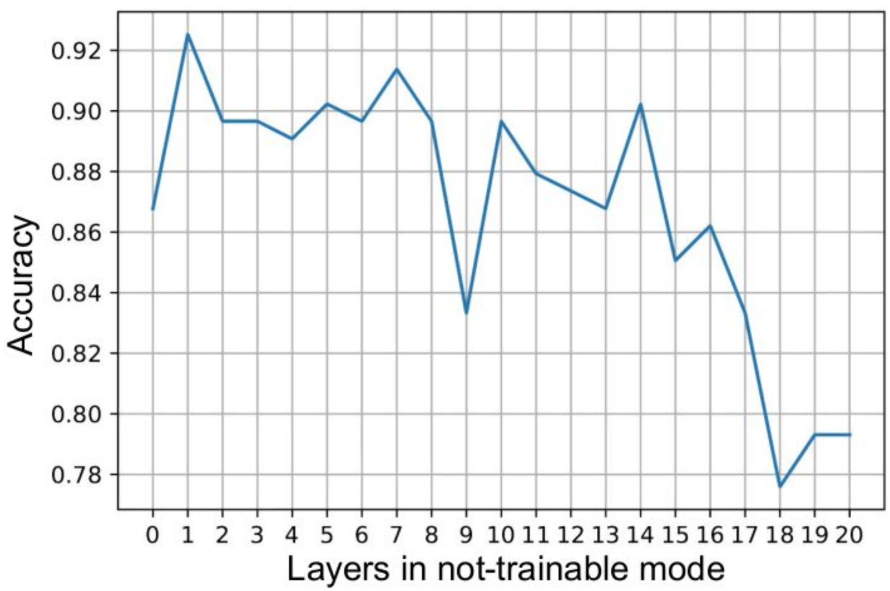

VGG19

ImageNet-trained CNN architectures

Databases:

Name	Glaucoma	Normal	Total
HRF	27	18	45
Drishti-GS1	70	31	101
RIM-ONE	194	261	455
sjchoi86-HRF	101	300	401
ACRIMA	396	309	705
Total	**788**	**919**	**1707**

ImageNet-trained CNN architectures

All these images were automatically cropped around the optic disc using a deep learning method[1]

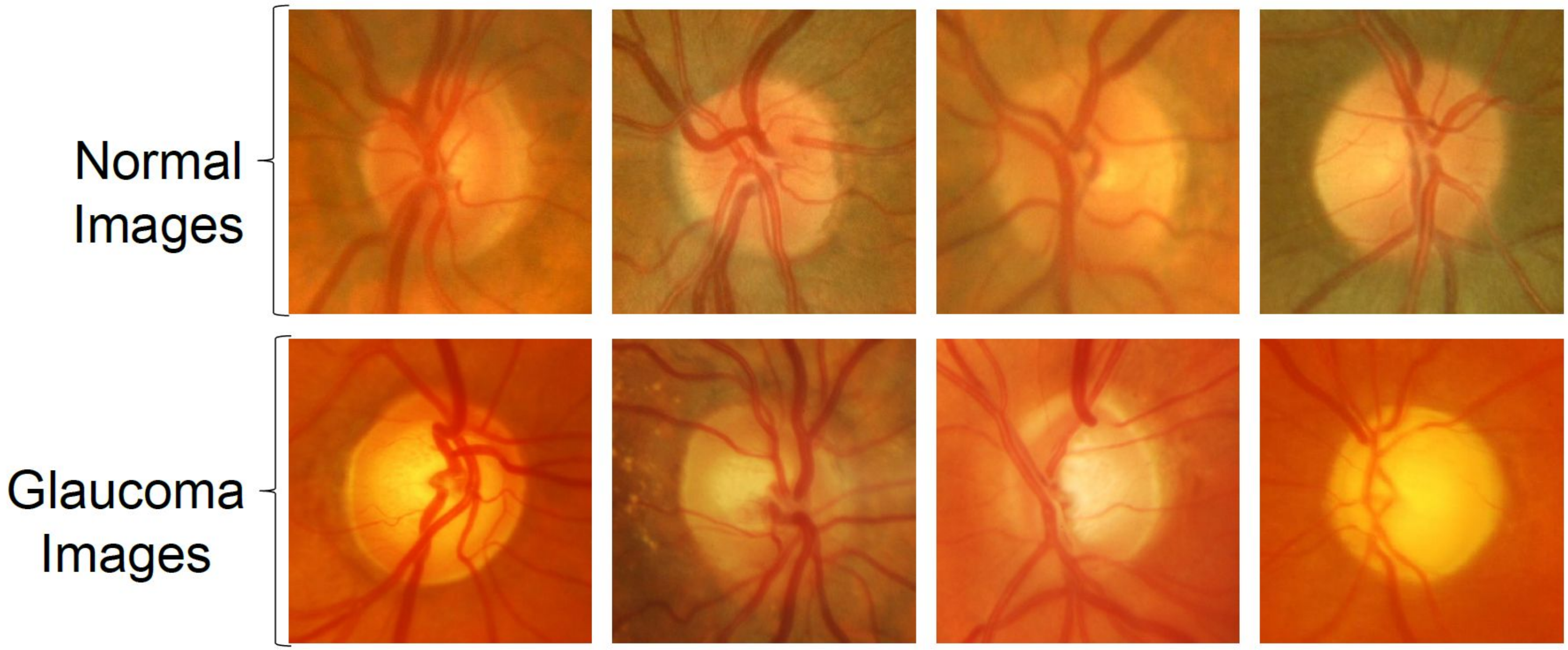

1) Xu P, Wan C, Cheng J, Niu D, Liu J. Optic disc detection via deep learning in fundus images. Fetal, infant and ophthalmic medical image analysis.

ImageNet-trained CNN architectures

- **Images were re-scaled:**

  224x224 px ⟶ VGG16, VGG19 and ResNet50
  299x299 px ⟶ InceptionV3 and Xception

- **We also used data augmentation**

  image rotations, image mirroring, shape deformation, vertical and horizontal flips.

- **10-fold cross-validation**

- **Cross-testing setting**

ImageNet-trained CNN architectures

Results 10-fold cross-validation:

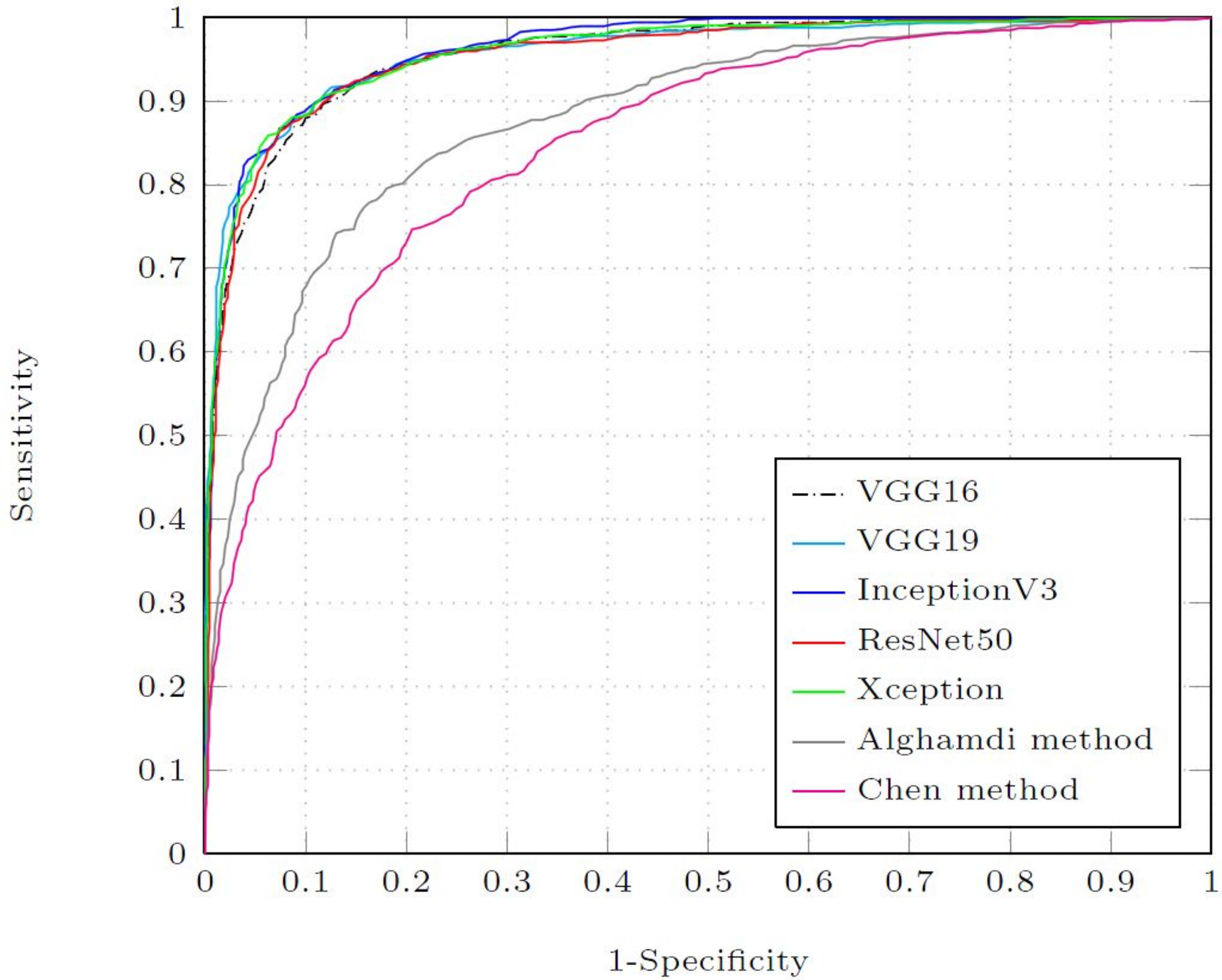

ImageNet-trained CNN architectures

Results 10-fold cross-validation:

Model Name	AUC	Accuracy	F-score	# parameters (in millions)
VGG16	0.9632	0.8948	0.9005	138
VGG19	0.9686	0.9069	0.9125	144
InceptionV3	0.9653	0.9000	0.9056	23
ResNet50	0.9614	0.9029	0.9076	25
Xception	0.9605	0.8977	0.9051	22

ImageNet-trained CNN architectures

Right predictions

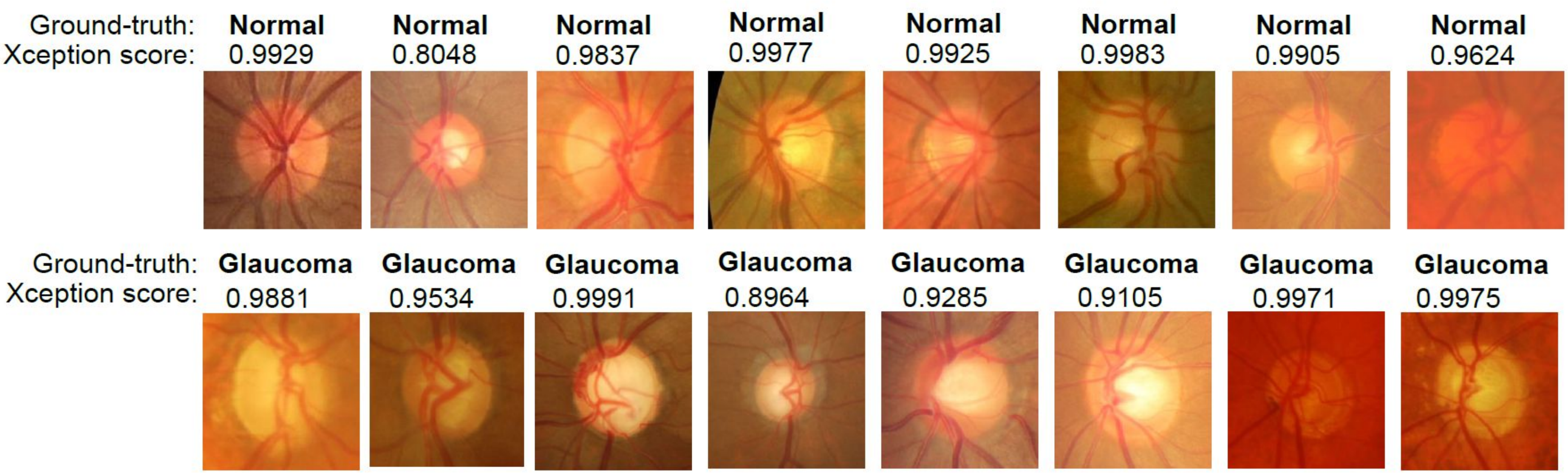

ImageNet-trained CNN architectures

Wrong predictions

Ground-truth:	**Normal**	**Normal**	**Normal**	**Normal**	**Normal**	**Normal**	**Normal**	**Normal**
Xception score:	0.0126	0.0799	0.3412	0.1306	0.1822	0.4173	0.2834	0.3487

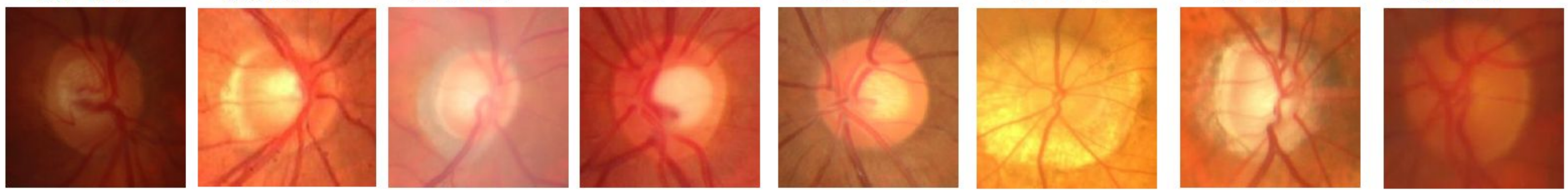

Ground-truth:	**Glaucoma**	**Glaucoma**	**Glaucoma**	**Glaucoma**	**Glaucoma**	**Glaucoma**	**Glaucoma**	**Glaucoma**
Xception score:	0.1252	0.2853	0.1273	0.0769	0.0858	0.3459	0.1270	0.3703

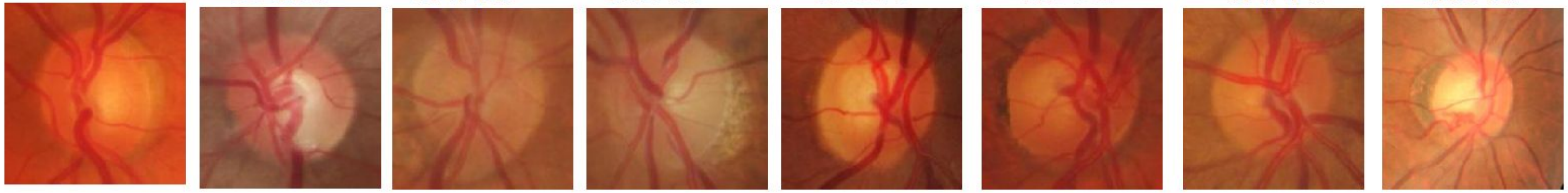

ImageNet-trained CNN architectures

Results cross-testing setting:

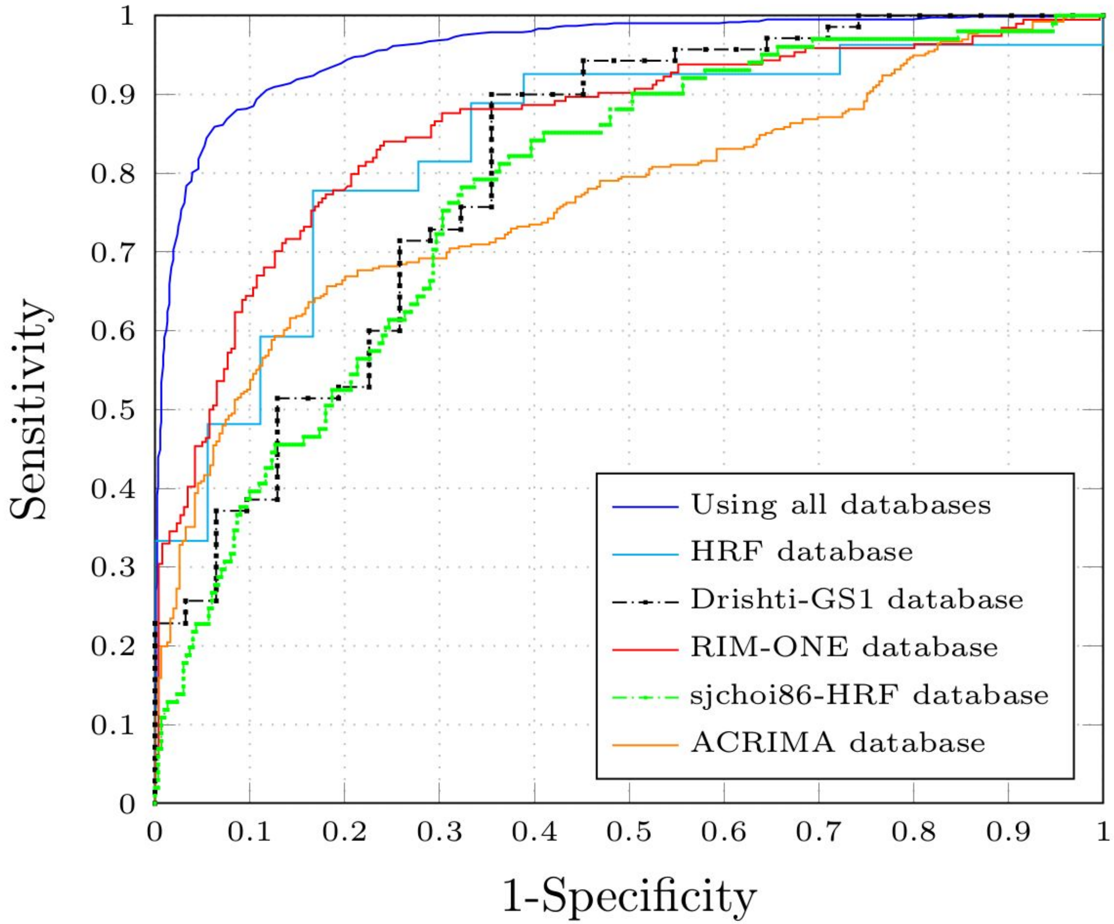

ImageNet-trained CNN architectures

Results cross-testing setting:

Database	AUC	Accuracy	# images
HRF	0.8354	0.8000	45
Drishti-GS1	0.8041	0.7525	101
RIM-ONE	0.8575	0.7121	455
sjchoi86-HRF	0.7739	0.7082	401
ACRIMA	0.7678	0.7021	705
Chen method	0.8310	NA	650
Alghamdi	NA	0.9214	2858

Outline

1. Introduction
2. Segmentation Methods
3. **Classification Methods**
   - ImageNet-trained CNN architectures
   - **Ensemble Setting with CNNs**
   - Conclusions
4. Image synthesis
5. Conclusions

Ensemble Setting with CNNs

Ensemble setting reduces the testing error

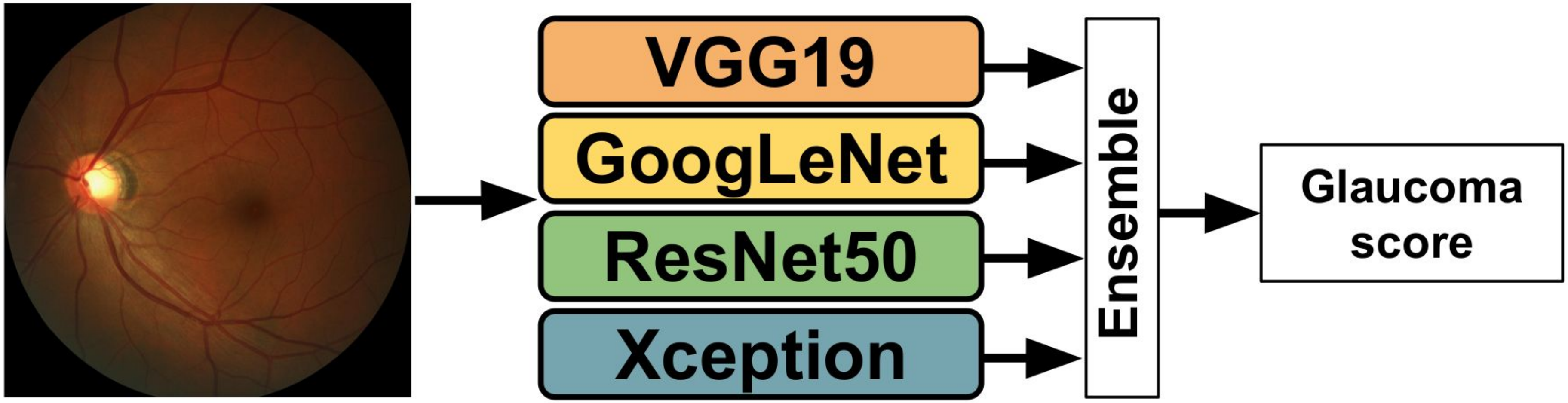

Ensemble Setting with CNNs

- **Images were re-scaled** to 256x256 px

- **Data augmentation**
  image rotations, image mirroring, shape deformation, vertical and horizontal flips.

- **Data was balanced** using the Synthetic Minority **Oversampling Technique** (SMOTE) on the training set of the REFUGE database.

Ensemble Setting with CNNs

Databases

Name	**Total**
HRF	30
Drishti-GS1	101
RIM-ONE v3	159
ORIGA-light	650
REFUGE	1200
Total	**2140**

An AUC of **0.94** was obtained for this task

Ensemble Setting with CNNs

Classification Leaderboard

Leaderboard sorted according to AUC

Leaderboard	Team	AUC	Reference Sensitivity
1	SMILEDeepDR	0.970763889	0.95
2	VRT	0.965972222	0.925
3	Winter_Fell	0.963576389	0.975
4	Masker	0.963055556	0.9
5	Needylove	0.963055556	0.9
6	BMIT	0.95125	0.899193548
7	Arunava	0.946111111	0.9
8	JULY	0.939513889	0.908189655
9	Cvblab	0.939201389	0.832317073
10	SDSA	0.935763889	0.781944444
11	NKSG	0.932777778	0.825
12	alchemist	0.9321875	0.832142857
13	CUMED	0.917916667	0.84244186
14	SDSAIRC	0.914826389	0.9
15	Mammoth	0.913125	0.884615385
16	BUCT	0.900069444	0.825
17	shanghaitech	0.889791667	0.8
18	INESC	0.871944444	0.75
19	SIAT-MMLab	0.87	0.75
20	MindLab	0.868368056	0.772727273
21	AIML	0.865069444	0.725
22	MIRL	0.856458333	0.748076923
23	xuhuaren	0.8478125	0.745454545
24	NightOwl	0.831979167	0.744224924
25	ImsightMedical	0.804583333	0.584375
26	PetuumCV	0.64375	0.396619718
27	BII	0.638125	0.353571429

Outline

1. Introduction
2. Segmentation Methods
3. **Classification Methods**
   - ImageNet-trained CNN architectures
   - Ensemble Setting with CNNs
   - **Conclusions**
4. Image synthesis
5. Conclusions

Conclusions

- Automatic glaucoma assessment using pretrained ImageNet CNN architectures were proposed.
- Obtained results showed this method outperforms the state-of-the-art.
- Deep tuning performs better than shallow tuning on these networks.
- Although performance is high, cross-testing results showed there is still a limitation when trying to generalise.
- To participate in the REFUGE challenge an ensemble setting was proposed.

Outline

1. Introduction
2. Segmentation Methods
3. Classification Methods
4. **Image synthesis**
   - **Using VAE and DCGAN**
   - Semi-supervised Learning using DCGAN
   - Conclusions
5. Conclusions

Image synthesis

Reasons

- Very limited data
- Use to generalise automatic glaucoma assessment methods

Using VAE and DCGAN

The Variational Autoencoder (VAE)[1] is composed by

- Approximate inference network (or encoder)
- Decoder network

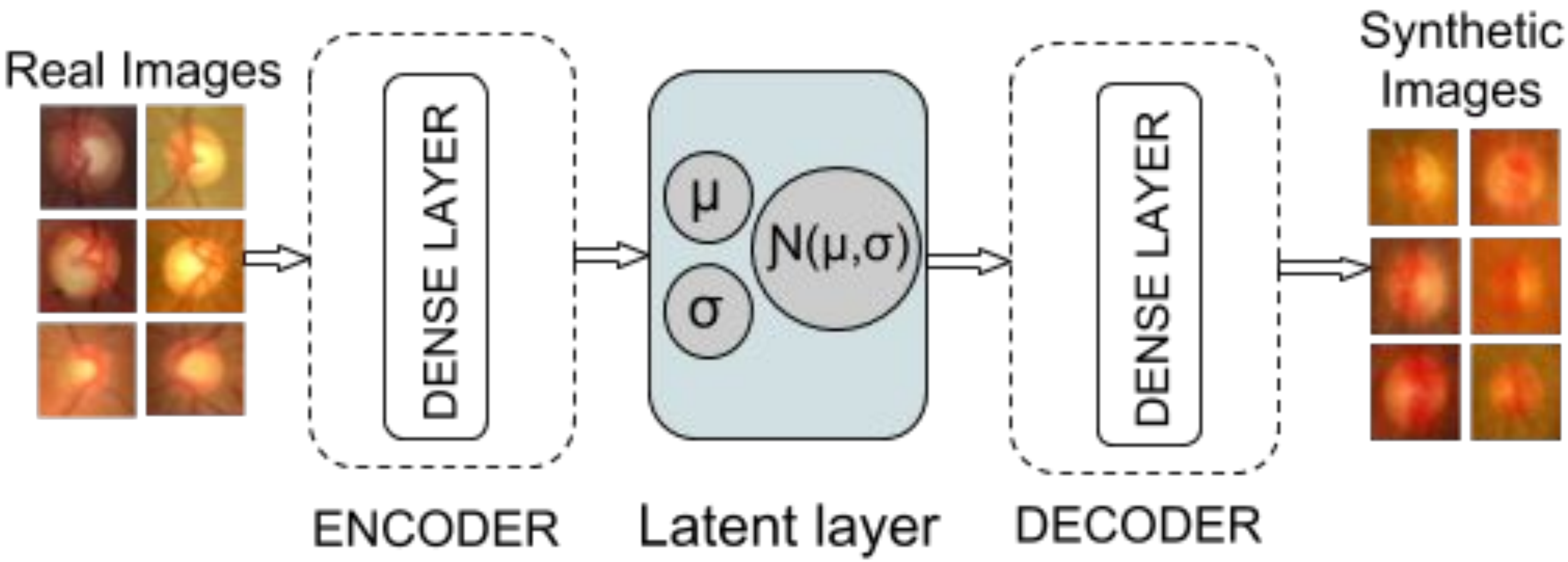

1 **Auto-Encoding Variational Bayes.** Diederik P Kingma, Max Welling
- http://kvfrans.com/variational-autoencoders-explained/

Using VAE and DCGAN

Differences between VAE and standard autoencoder:

- **Latent variables follow a unit gaussian distribution**

- **Loss function composed of separate losses:**

  The generative loss → Mean squared error that measures how accurately the network reconstructed the images

  Latent loss → Kullback Leibler divergence that measures how closely the latent variables match a unit gaussian.

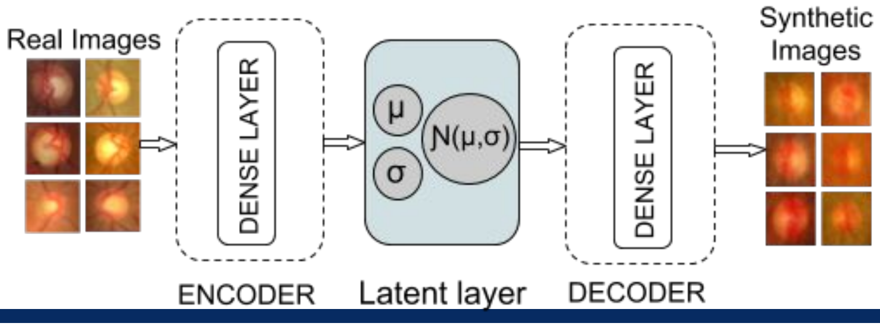

Using VAE and DCGAN

The Deep Convolutional Generative Adversarial Network (DCGAN)[1].

- It also consists of two networks, the generator and discriminator.
- A major improvement on the first GAN.

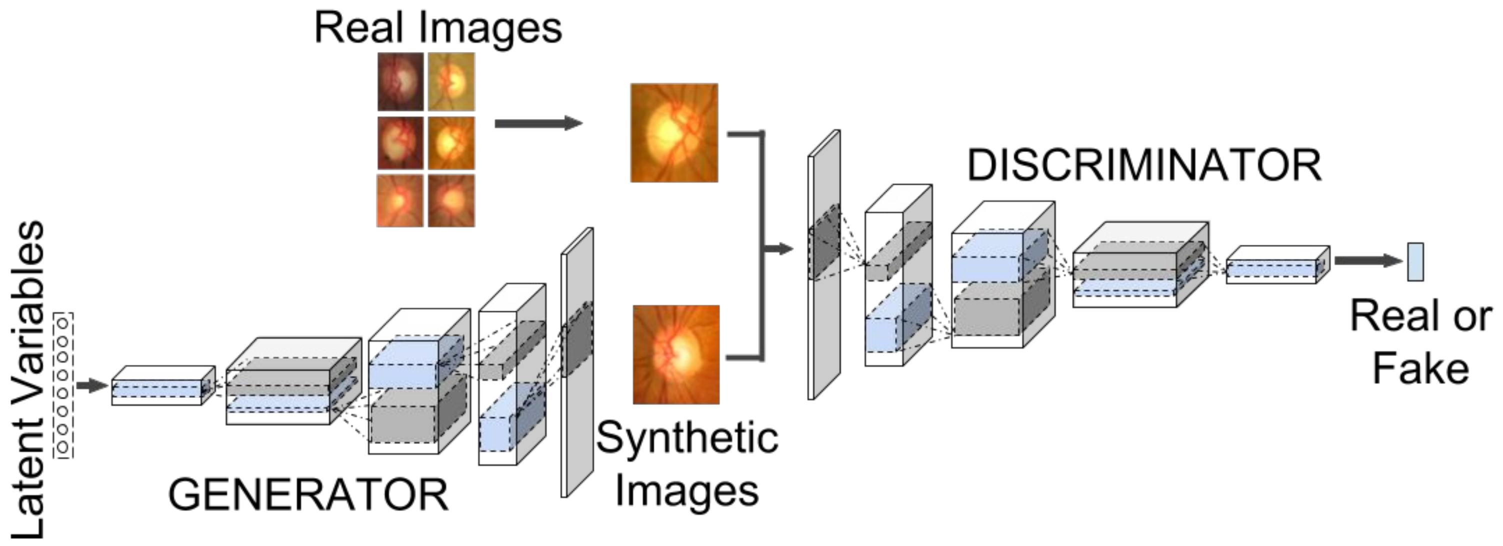

1 Unsupervised Representation Learning with Deep Convolutional Generative Adversarial Networks.
Alec Radford, Luke Metz, Soumith Chintala

Using VAE and DCGAN

- **Analysed resolutions** 28x28 pix, 56x56 pix, 112x112 pix and 224x224 pix.
- **Latent space** From 32 to 100 latent variables (multivariate Gaussian).

Using VAE and DCGAN

Databases

Name	Total
HRF	45
Drishti-GS1	101
ORIGA-light	650
RIM-ONE	455
sjchoi86-HRF	401
ACRIMA	705
Total	**2357**

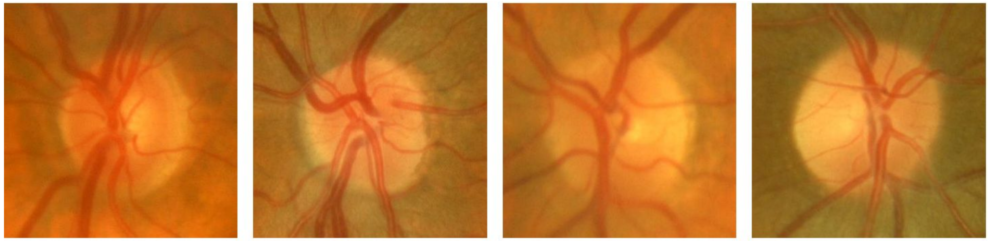

Cropped images

Xu P, Wan C, Cheng J, Niu D, Liu J. Optic disc detection via deep learning in fundus images. Fetal, infant and ophthalmic medical image analysis.

Using VAE and DCGAN

Results VAE: **100 latent variables**

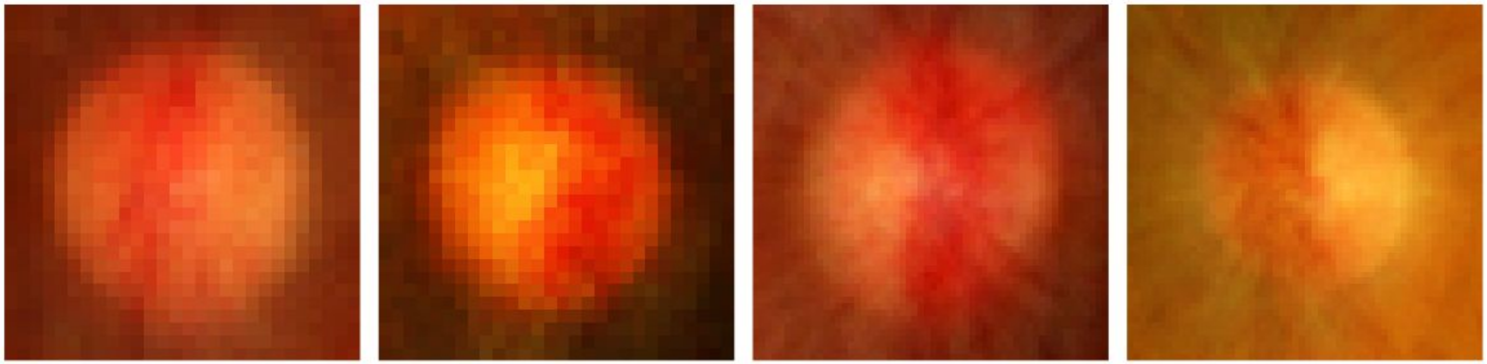

28x28 px 56x56 px

Results DCGAN: **100 latent variables**

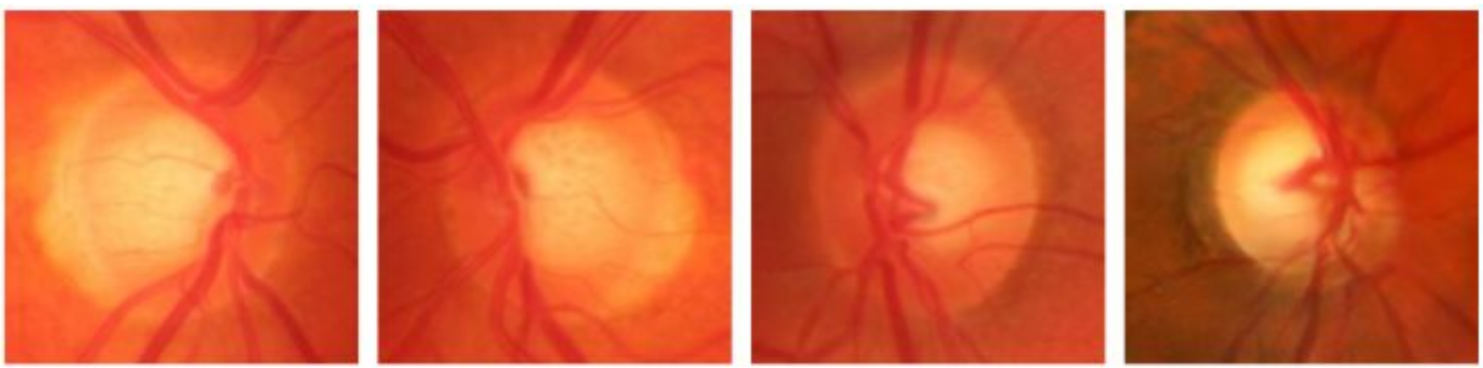

224x224 px

Using VAE and DCGAN

For qualitative and quantitative evaluation, 100 synthetic images and 100 real images were selected

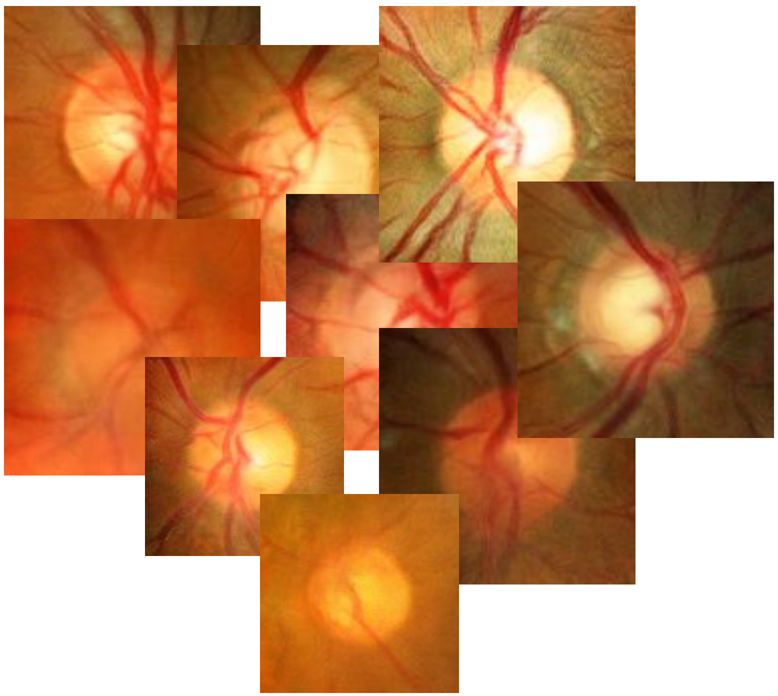

Synthetic images

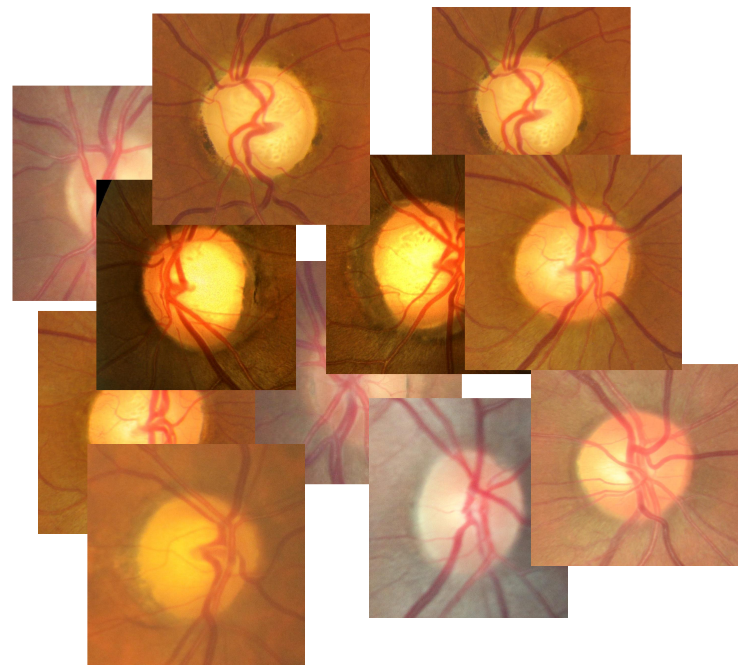

Real images

Using VAE and DCGAN

Qualitative evaluation

1/200

Fake or real?

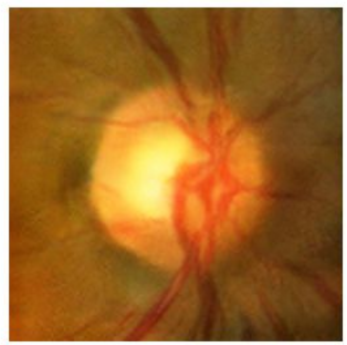

Fake Real

Press here to quit the validation

Web App: https://cvblab.synology.me/ganval/index.php

Using VAE and DCGAN

Results qualitative evaluation DCGAN images

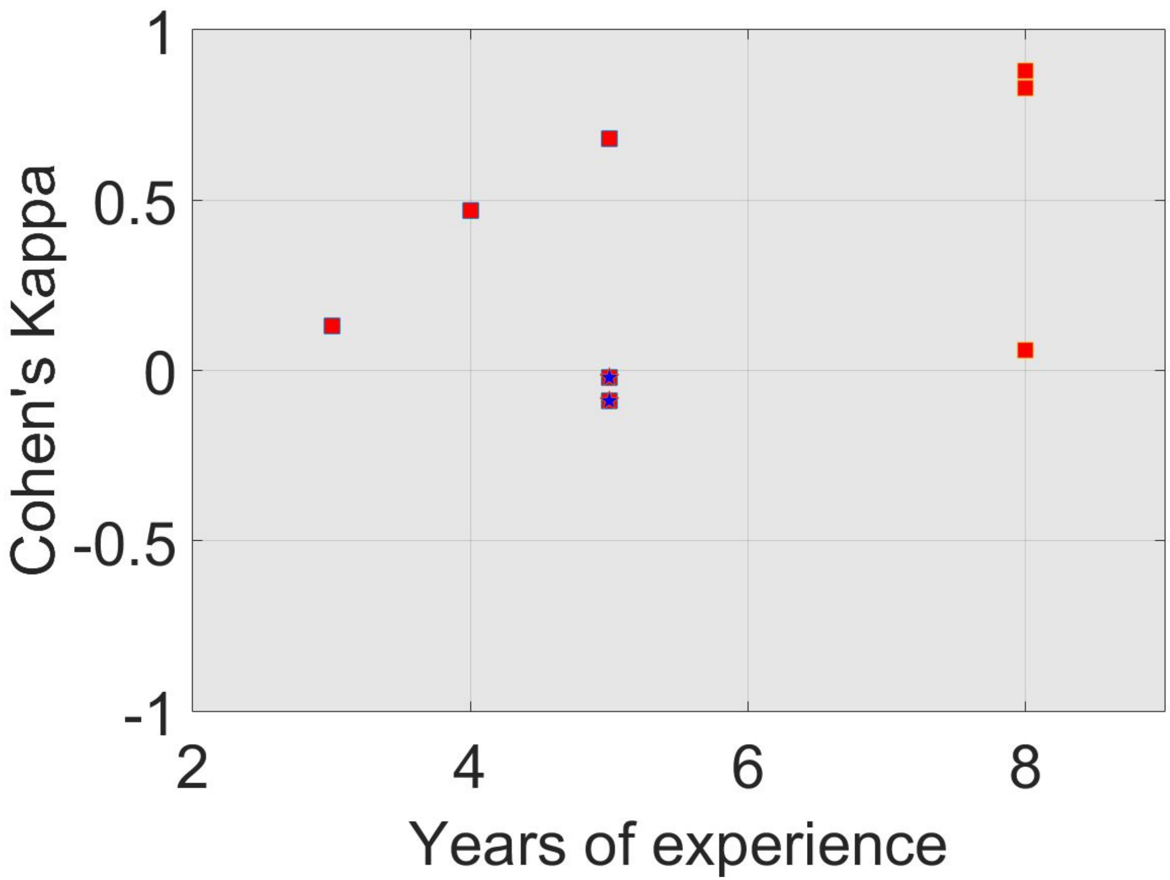

Ten experts with 3 to 8 years of experience

Cohen's kappa

- 0 represents random chance
- 1 represents a perfect agreement between the ground-truth and the expert.

Using VAE and DCGAN

Results quantitative evaluation DCGAN and Real images: 2D-histograms[1]

Average 2D-histograms: RGB channels normalized by the luminance

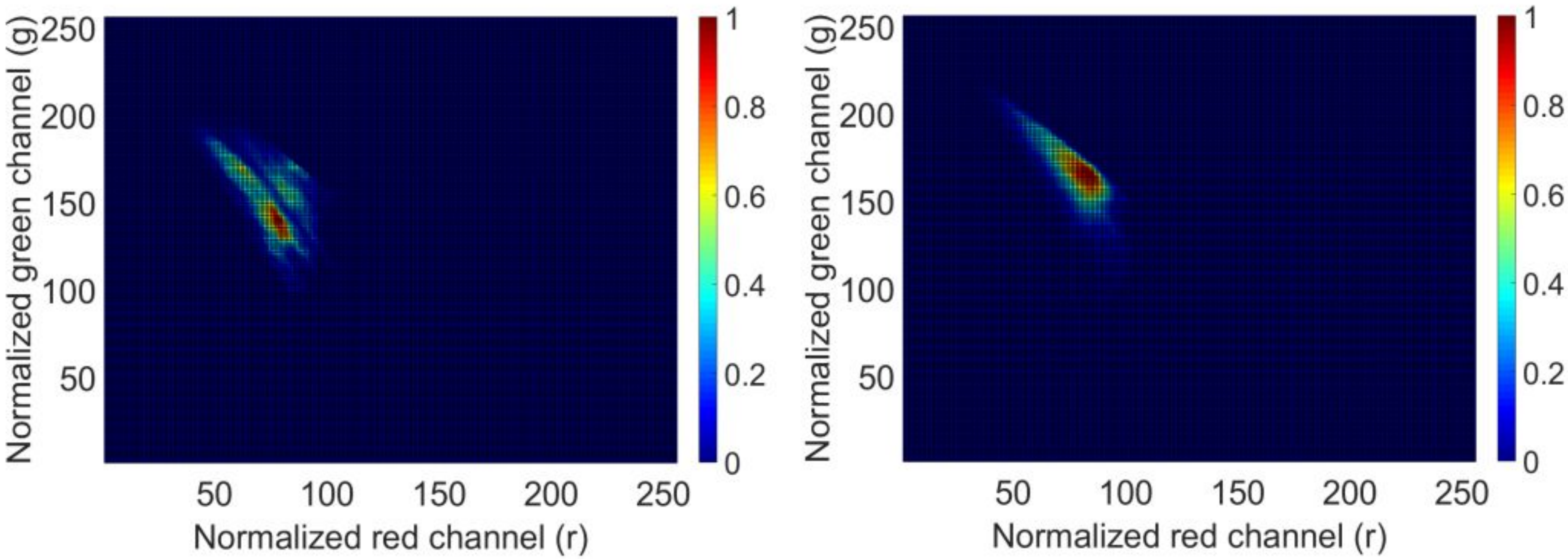

DCGAN images *Real images*

1 Adrian Colomer et al., Colour normalization of fundus images based on geometric transformations applied to their chromatic histogram.

Using VAE and DCGAN

Results quantitative evaluation DCGAN and Real images:

Average and standard deviation of the mean-squared error

Average 2D-histogram	**Real Images**	**Synthetic Images**
Real	0.0028 (0.000325)	0.0036 (0.000543)
Synthetic	**0.0031 (0.000461)**	0.0022 (0.000562)

Using VAE and DCGAN

Results quantitative evaluation DCGAN and Real images:

Average vessel, Optic Disc and Background proportion

	Synthetic Images	Real Images
Vessel proportion[1]	0.1431 (0.0306)	0.1519 (0.0306)
Optic Disc proportion	0.1776 (0.0339)	0.2456 (0.0722)
Background	0.6792 (0.0428)	0.6025 (0.0795)

Quality evaluation of synthetic images should be specific for each application[2]!

1 Sandra Morales et al., Computer-Aided Diagnosis Software for Hypertensive Risk Determination Through Fundus Image Processing.
2 L Theis et al., A note on the evaluation of generative models.

Outline

1. Introduction
2. Segmentation Methods
3. Classification Methods
4. **Image synthesis**
   - Using VAE and DCGAN
   - **Semi-supervised Learning using DCGAN**
   - Conclusions
5. Conclusions

Semi-supervised Learning using DCGAN

- **We trained the DCGAN as image synthesizer and as semi-supervised learning method**

- **Using semi-supervised learning better classifier can be built with a large amount of unlabelled data and small set of labelled data**

Semi-supervised Learning using DCGAN

SS-DCGAN architecture

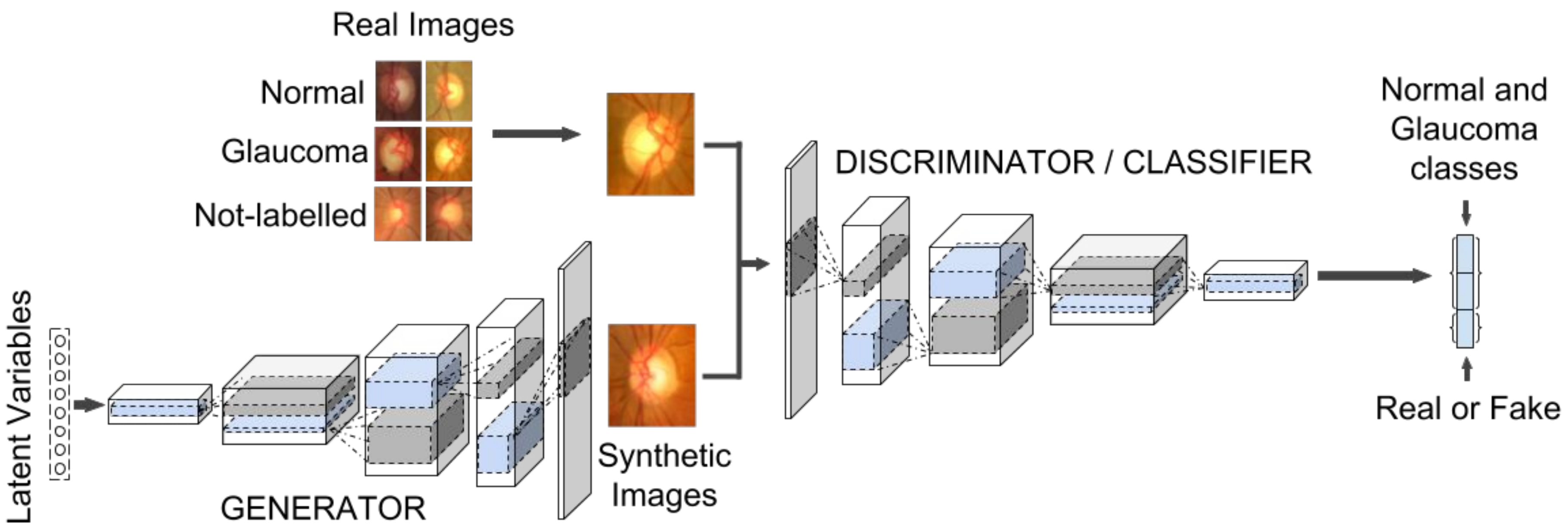

Semi-supervised Learning using DCGAN

Unlabeled databases

Database	Total
DRIVE	40
MESSIDOR	1200
DR KAGGLE	82447
STARE	195
e-ophtha	431
ONHSD	89
CHASEDB1	28
DRIONS-DB	105
SASTRA	34
Total	**84569**

Labeled databases

Database	Total
ORIGA-light	650
Drishti-GS1	101
RIM-ONE	455
sjchoi86-HRF	401
HRF	45
ACRIMA	705
Total	**2357**

Semi-supervised methods usually perform better than supervised.

X. Zhu, Semi-Supervised Learning Literature Survey, Computer Sciences, University of Wisconsin-Madison, Tech. Rep. 1530, 2005

Semi-supervised Learning using DCGAN

DCGAN spherical interpolation

$$slerp(z_1, z_2, t) = \frac{sin((1-t)\theta)}{sin(\theta)} z_1 + \frac{sin(t\theta)}{sin(\theta)} z_2$$

Spherical Interpolation (slerp)

$t \longrightarrow$ A value between 0 and 1.
When t=0, slerp = Z_1 whereas t=1, slerp = Z_2

$\theta \longrightarrow$ Angle between Z_1 and Z_2

Semi-supervised Learning using DCGAN

DCGAN spherical interpolation: Results for 100 latent variables

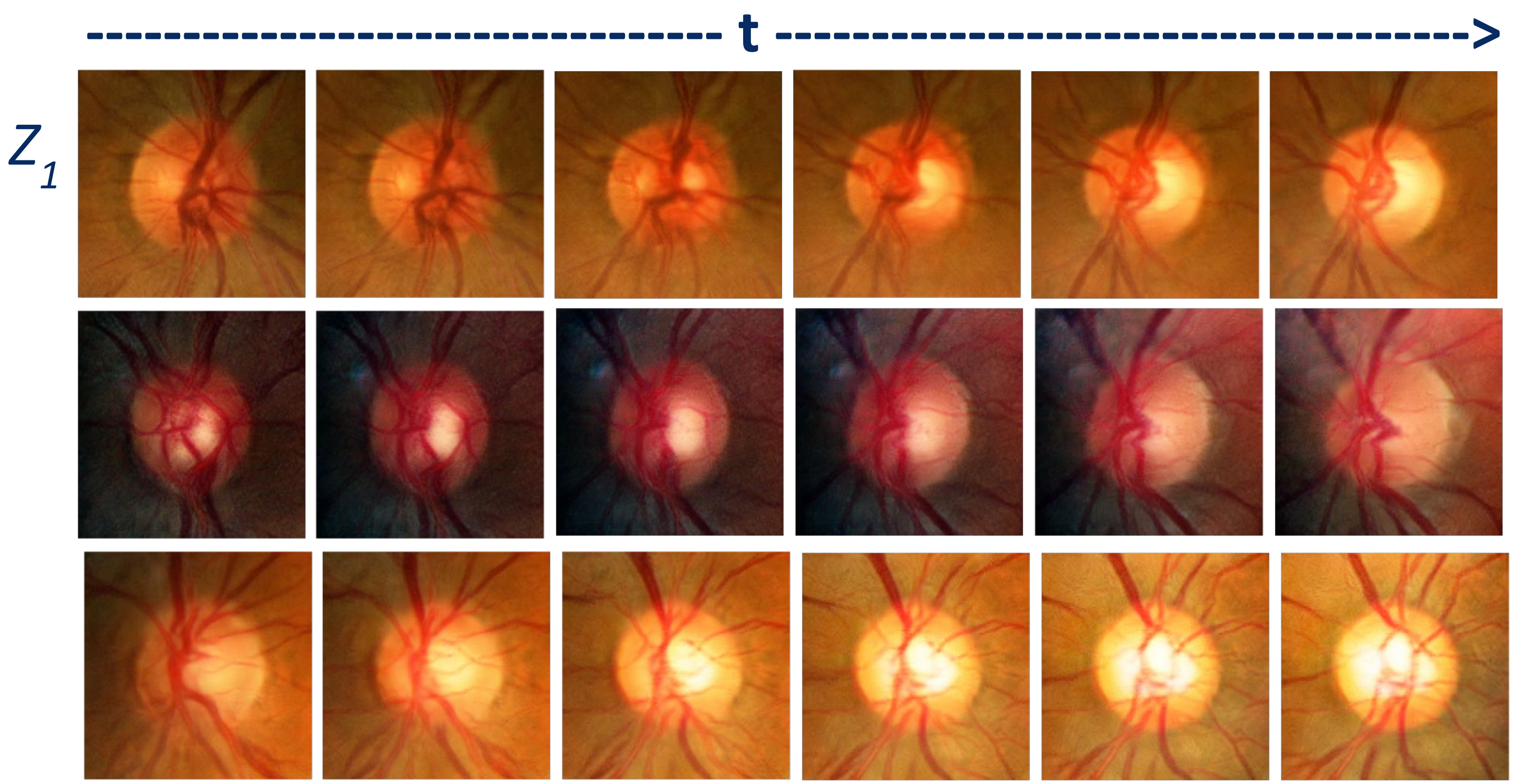

The latent space did NOT memorise the training set

Semi-supervised Learning using DCGAN

DCGAN, SS-DCGAN and Costa’s method

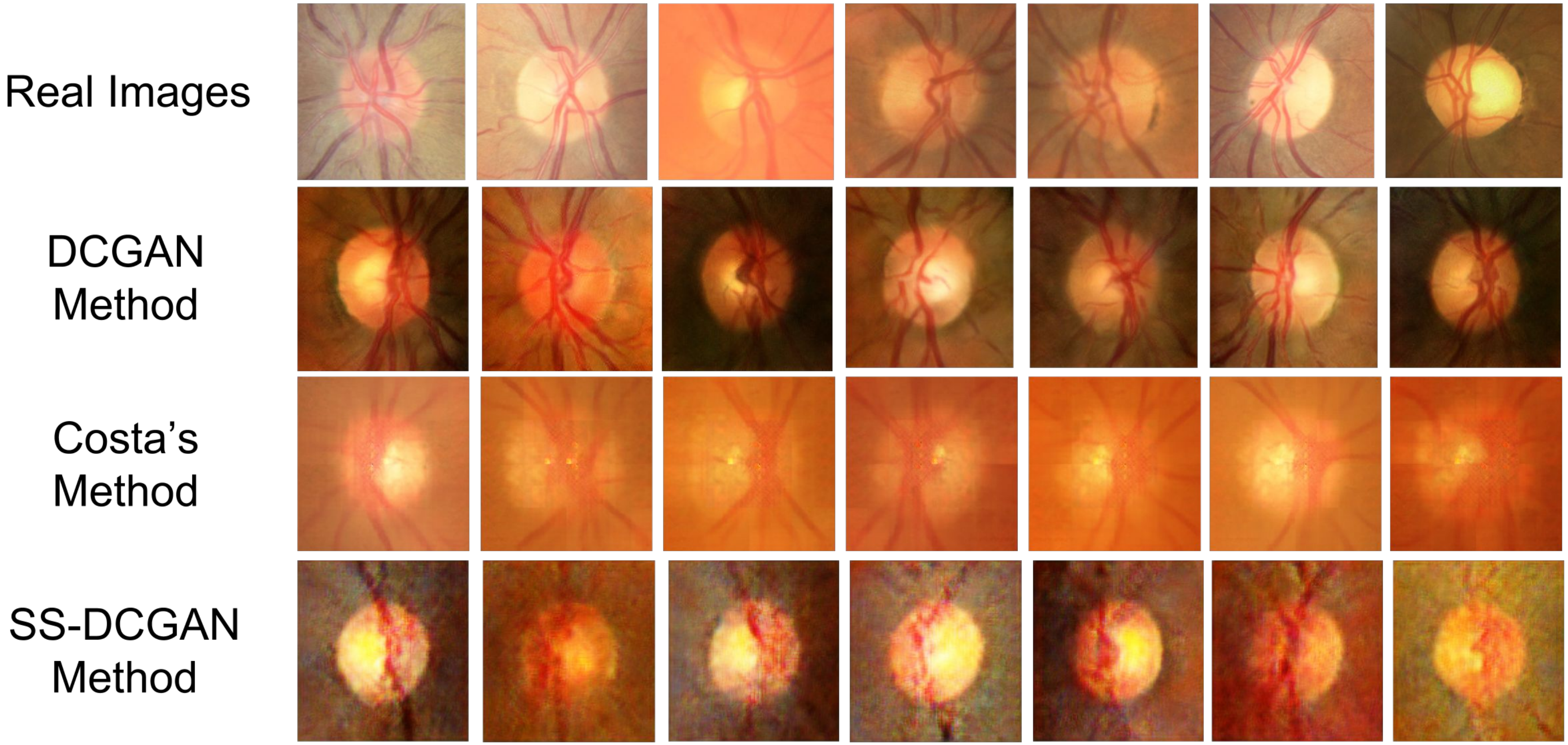

Semi-supervised Learning using DCGAN

DCGAN generates better images

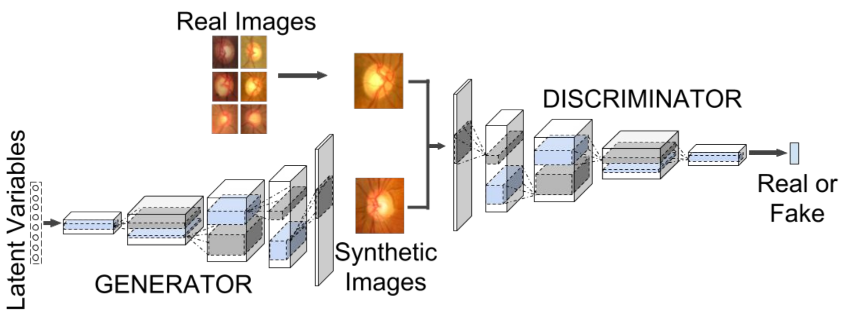

We train both DCGAN and SS-DCGAN!

SS-DCGAN trains a better classifier

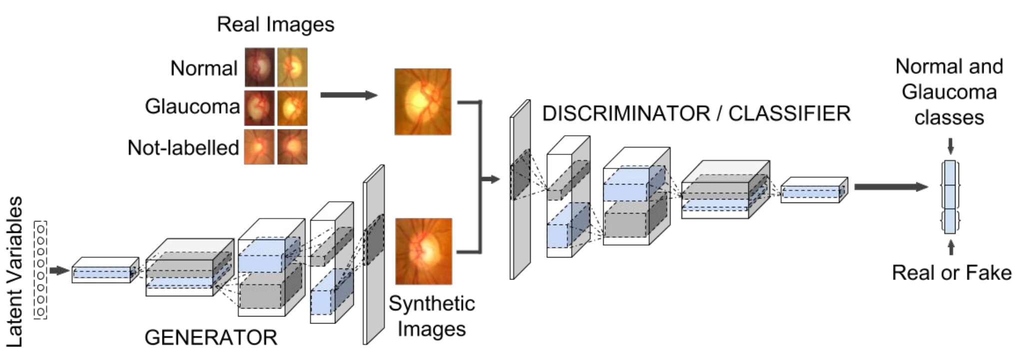

Using VAE and DCGAN

For qualitative and quantitative evaluation, 100 DCGAN images, 100 Costa's images and 100 real images were selected

DCGAN images

Costa's images

Real images

Semi-supervised Learning using DCGAN

Qualitative evaluation using t-SNE

100 features extracted from the ResNet50 trained on ORIGA-light

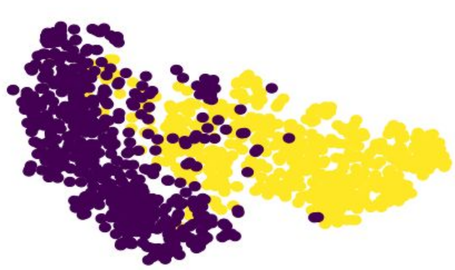

DCGAN images

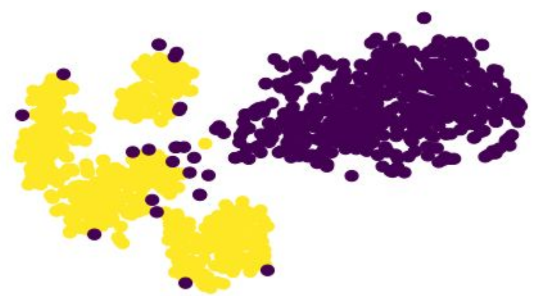

Costa's images

Yellow dots represent the features extracted from the real images

t-SNE stands for **t-Distributed Stochastic Neighbor Embedding**. It is a technique for dimensionality reduction that is particularly well suited for the visualization of high-dimensional datasets

Semi-supervised Learning using DCGAN

Quantitative evaluation: Average 2D-histograms

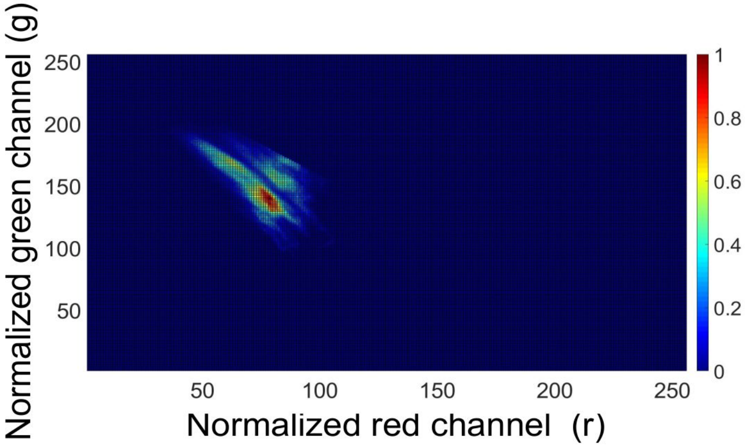

DCGAN images

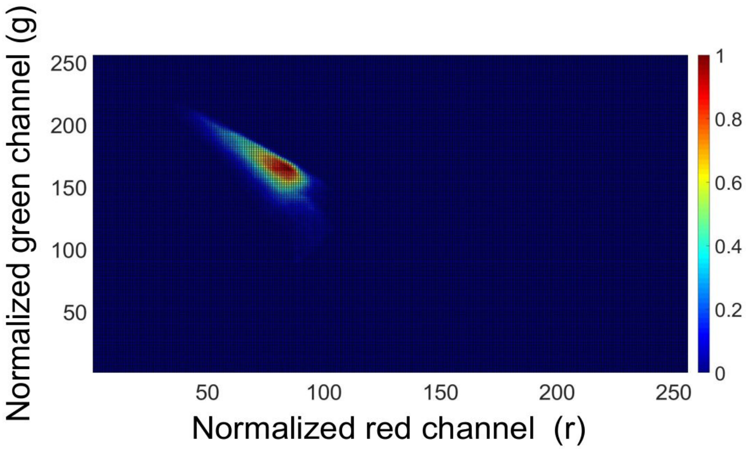

Real images

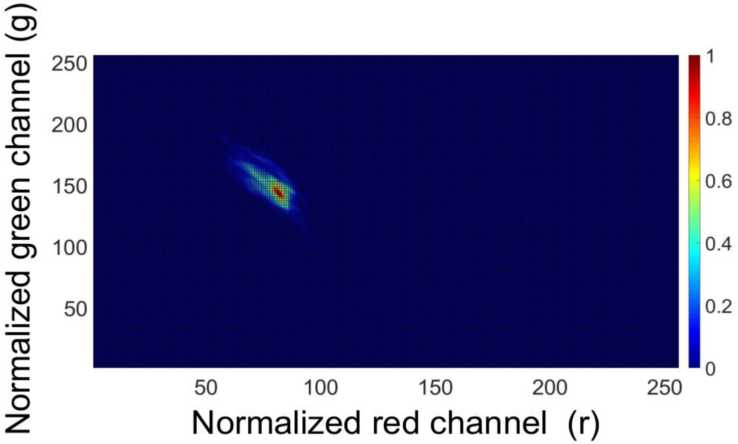

Costa's images

Semi-supervised Learning using DCGAN

Quantitative evaluation

Average and standard deviation of the mean-squared error

Average 2D-histogram	**Real Images**	**DCGAN method**	**Costa's method**
Real	0.0028 (0.000325)	0.0036 (0.000543)	0.0013 (0.000262)
DCGAN method	**0.0031 (0.000461)**	0.0022 (0.000562)	0.0016 (0.000439)
Costa's method	**0.0031 (0.000126)**	0.0035 (0.000178)	0.0010 (0.000163)

Semi-supervised Learning using DCGAN

Quantitative evaluation: *Vessel, Optic Disc and background proportion*

	Real Images	DCGAN Images	Costa's method
Vessel proportion	**0.1519 (0.0306)**	**0.1431 (0.0306)**	**0.1026 (0.0195)**
Optic Disc proportion	0.2456 (0.0722)	0.1776 (0.0339)	0.1851 (0.0396)
Background	0.6025 (0.0795)	0.6792 (0.0428)	0.7122 (0.0437)

Real sample

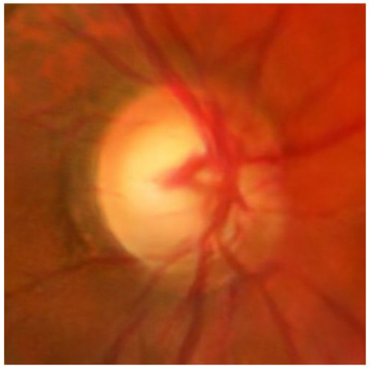

DCGAN sample

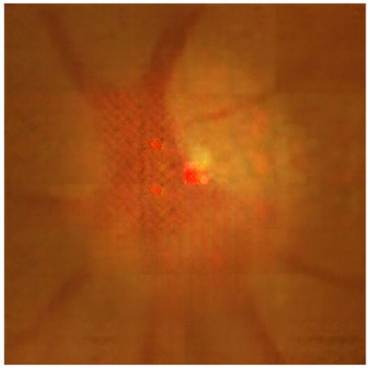

Costa's sample

Semi-supervised Learning using DCGAN

Results glaucoma classifier using SS-DCGAN

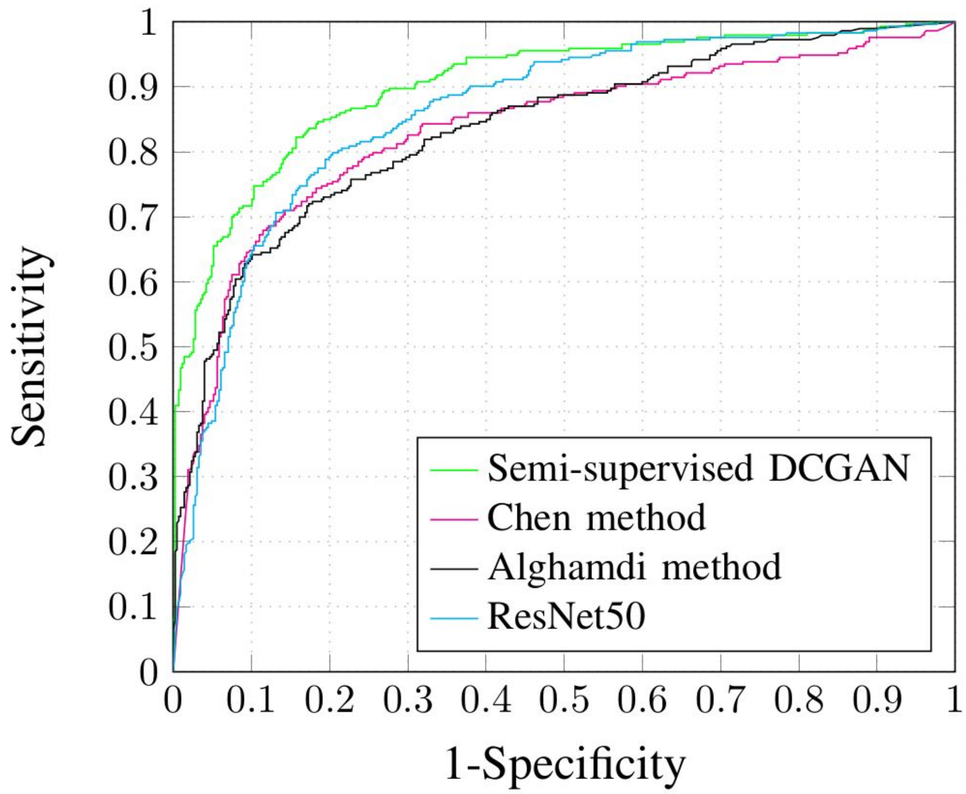

Model	AUC
Chen	0.8330
Alghamdi	0.8365
ResNet50	0.8607
SS-DCGAN	**0.9017**

Outline

1. Introduction
2. Segmentation Methods
3. Classification Methods
4. **Image synthesis**
   - Using VAE and DCGAN
   - Semi-supervised Learning using DCGAN
   - **Conclusions**
5. Conclusions

Conclusions

- DCGAN performs better as image synthesizer than the VAE architecture

- DCGAN generates better quality images than the Costa's method.
  Previous vessel segmentation is not needed as in Costa's method.

- SS-DCGAN doesn't generate better synthetic images than DCGAN but its strength relies on the glaucoma classifier.

Outline

1. Introduction
2. Segmentation Methods
3. Classification Methods
4. Image synthesis
5. **Conclusions**

Conclusions

Segmentation

- A novel optic cup segmentation method based on the stochastic watershed transformation.
- It was presented why the U-Net performs better than traditional methods for optic disc and optic cup segmentation.

Conclusions

Segmentation

- **Diaz-Pinto A,** Morales S, Naranjo V, Alcocer P, Lanzagorta A. Glaucoma Diagnosis by Means of Optic Cup Feature Analysis in Color Fundus Images. 24th European Signal Processing Conference (EUSIPCO). August 2016.

- **Diaz-Pinto A,** Morales S, Naranjo V, Alcocer P, Lanzagorta A. Diagnóstico Automático del Glaucoma a través de la Segmentación y Análisis de la Copa Óptica Usando Imágenes de Fondo de Ojo. XXXIV Congreso Anual de la Sociedad Española de Ingeniería Biomédica. pp 383-386. 2016

- Vesal S, **Diaz-Pinto A,** Ravikumar N, Ellman S, Davari A, Maier A. Semi-Automatic Algorithm for Breast MRI Lesion Segmentation Using Marker-Controlled Watershed Transformation. Nuclear Science Symposium and Medical Imaging Conference. October 2017.

- **Diaz-Pinto A,** Morales S, Naranjo V, Navea A. Computer-aided Glaucoma Diagnosis using Stochastic Watershed Transformation on Single Fundus Images. Journal of Medical Imaging and Health Informatics. 2019

Conclusions

Classification

- Automatic glaucoma classification using convolutional neural networks (CNNs) pre-trained on the ImageNet database was proposed

- A method using four CNNs on an average ensemble setting was presented

Article:

- **Diaz-Pinto A,** Morales S, Naranjo V, Köhler T, Mossi J M, Navea A. CNNs for Automatic Glaucoma Assessment using Fundus Images: An Extensive Validation. BioMedical Engineering OnLine 2019 18:29, doi:10.1186/s12938-019-0649-y. 2019

Conclusions

Image synthesis

- Two image synthesizers based on the VAE and DCGAN architecture were analysed

- A semi-supervised learning method for automatic glaucoma assessment was presented

Conclusions

Image synthesis

- **Diaz-Pinto A**, Colomer A, Naranjo V, Morales S, Xu Y, Frangi A F. Retinal Image Synthesis and Semi-supervised Learning for Glaucoma Assessment. IEEE Transactions on Medical Imaging journal. doi:10.1109/TMI.2019.2903434. 2019

- **Diaz-Pinto A**, Colomer A, Naranjo V, Morales S, Xu Y, Frangi A F. Retinal Image Synthesis for Glaucoma Assessment using DCGAN and VAE Models, 19th International Conference on Intelligent Data Engineering and Automated Learning. Nov 2018. pp 224-232.

Thank you!

Andres Diaz-Pinto
a.diaz-pinto@leeds.ac.uk